

18 AFOSR TR-78-1506 19

LEVEL II

12

AD A061959

6 Final Scientific Report on  
OPTICAL DATA PROCESSING and STATISTICAL OPTICS  
Submitted by  
10 Nicholas George Principal Investigator  
Grant No. AFOSR-72-2234  
Caltech Engineering 136C-F49620-76-C-0021 (Account No. 61297)

California Institute of Technology

Pasadena, California 91125

9 Final report  
Period Covered: 1 July 1976 - 30 June 1978

Final Technical Report Due: 30 August 1978

15 F49620-76-C-0021, AFOSR-72-2234  
Prepared for

ELECTRONIC AND SOLID STATE SCIENCES

AIR FORCE OFFICE OF SCIENTIFIC RESEARCH (AFSC)

ARLINGTON, VIRGINIA 22209

16 3385  
17 B2

12 44P

11 Oct 78

DDC  
RECEIVED  
DEC 8 1978  
D

AIR FORCE OFFICE OF SCIENTIFIC RESEARCH (AFSC)  
NOTICE OF TRANSMITTAL TO DDC  
This technical report has been reviewed and is  
approved for public release in accordance with FAR 190-12 (7b).  
Distribution is unlimited.  
A. D. BLOSE  
Technical Information Officer

Approved for public release;  
distribution unlimited.

78-12 04-068

DDC FILE COPY

Final Scientific Report on  
OPTICAL DATA PROCESSING and STATISTICAL OPTICS

Nicholas George

ABSTRACT

This final scientific report contains a summary of research at Caltech on the wavelength sensitivity of speckle. Included in this bibliography are research publications by N. George, A. Jain, A. Livanos, R.D.S. Melville, C.H. Papas, and J. Roth. Topics in speckle supported under the subject contract are described: (1) diffraction by a serrated aperture and (2) propagation in an experimental test chamber containing a turbulent gaseous mixture.

Research on the fabrication of grating structures for use in integrated optics is also described. Chirped or variable period gratings have been successfully made by a holographic process. Briefly, a waveguiding layer of Corning 7059 glass is sputtered onto a substrate glass using the Technics MIM Model 5.5 ion-beam etching machine. Photoresist is coated onto the waveguiding layer, exposed holographically in an argon or helium-cadmium laser beam, developed and then ion-milled. Extensive theory and technique are reported in the bibliography of publications listed in this report.

ACCESSION for	
DTIC	White Section <input checked="" type="checkbox"/>
DDO	Dark Section <input type="checkbox"/>
UNANNOUNCED	<input type="checkbox"/>
JUSTIFICATION.....	
BY.....	
DISTRIBUTION/AVAILABILITY CODES	
Dist.	AVAIL. and/or SPECIAL
A	

Final Scientific Report on  
OPTICAL DATA PROCESSING and STATISTICAL OPTICS

Table of Contents

1. Introduction and Time Period
  2. Topics in Speckle
    - 2.1 Serrated Aperture
    - 2.2 Laser Propagation through a Turbulent Gaseous Mixture
    - 2.3 Cumulative Listing of Publications on Speckle
  3. Photoresist Techniques for Integrated Optics
    - 3.1 Introduction
    - 3.2 Listing of Publications
    - 3.3 Appended Publications
  4. Personnel Supported under the Subject Contract
- DD 1473 Form

Final Scientific Report on  
OPTICAL DATA PROCESSING and STATISTICAL OPTICS

Nicholas George, Principal Investigator

1. Introduction and Time Period

This report describes a program of research in two main areas of modern optics: Sec. 2. Topics in Speckle and Sec. 3. Photoresist Techniques for Integrated Optics. The main portions of research supported under the subject contract were conducted during the period from 1 July 1976 to 30 June 1977; however a no-cost extension of the contract date was requested from 30 June 1977 to 30 June 1978.

2.0 Topics in Speckle

The study of speckle is basically a combining of ideas in communication theory with those in electromagnetics in order to set quantitative limits on the performance of general optical configurations. In essence, it is a study of noise and resolution. In comparing the working resolution of single color systems to white light systems, it is immediately evident that with diffuse objects the latter illumination is considerably easier to manage. The reason for this is the deleterious speckle noise which occurs with the use of monochromatic light. With multi-color lasers, we have shown that the effect of speckle can be essentially eliminated; and thus the performance of systems with this type of illumination is competitive with white light insofar as resolution and superior both in terms of brightness and in the application of Fourier optical methods. The general trend of our studies in speckle has shifted now to the consideration of the questions: "In what ways,

if any, can one achieve better performance using separate multiple tones from a laser rather than white light? What method for combining single-tone images is optimum in regard to image quality and resolution?" Coupling of microscopes or any imaging optics to tiny photodiode arrays, thence to electronic digital computers, seems the logical way to study the various correlation possibilities which may ultimately lead to substantial advancements over current methods.

A complete bibliography of the speckle publications by the Principal Investigator and his colleagues is given in Sec. 2.3. Since this is a final technical report and further effort is not planned, it was felt appropriate to provide a comprehensive listing of the speckle publications which resulted from contractual support by the U.S. Air Force Office of Scientific Research. However, it is emphasized that this listing includes research completed prior to the period of the subject report. The topics detailed in Sections 2.1 and 2.2 are speckle research supported under the subject contract period.

## 2.1 Serrated Aperture (N. George and G.M. Morris)

A new class of diffraction theory problems has been studied. In these an aperture with a rough or serrated edge is considered. This is in contrast to the usual speckle problem in which longitudinal phase variations cause perturbations in the phase front, i.e., the diffuser problem. It is also different from the usual blackbody radiator problem, where finite correlation lengths of the aperture illumination are the essence of the problem.

Under the subject contract, we studied the roughened edge in considerable detail. While this is only one example, it was felt to be of special interest as a building block in image quality studies. Also because of our interest in diffraction pattern sampling and hybrid (opto-electronic) computers, it was felt desirable to consider first the problem of finding the optical transform of a serrated edge. For this problem, we obtained a closed form solution for the second order moment of the electric field in the transform plane. As first derived, this correlation function did not include wavelength variation; but more recently the analysis has been generalized to include wavelength dependence. A first report of the analysis together with some experiments using razor blades roughened with emery paper was presented at the 1977 Annual Meeting of the Optical Society of America. The abstract of the presentation follows:<sup>+</sup>

TK17. Randomly Serrated Edges, Lines, and Apertures.\*  
 NICHOLAS GEORGE AND G. M. MORRIS,† *The Institute of Optics, University of Rochester, Rochester, N.Y. 14627.*—In automatic pattern recognition, film grain noise and other image-quality degradation can give rise to characteristic optical transforms which are readily sampled. Related to this interest, a new class of diffraction-theory problems has been analyzed. As a simple first step, we calculate the optical transform, as well as the Fresnel zone pattern, for a serrated edge. The edge roughness is described by a second-order density and its associated characteristic function. For convergent monochromatic illumination, we derive an expression for the output electric field and for the second-order correlation function in terms of output position, wavelength offset, edge roughness, and correlation length. The effect of the serration is to distribute the energy in the transform plane; the large central spike, characteristic of an edge, is greatly suppressed. Theoretical results are also presented for other serrated apertures. As the roughness increases, the general trend is to trade the regular interference ringing for a speckle pattern. Wavelength-sensitivity experiments are described for these serrated apertures, using a tunable dye laser and computer-generated patterns of controlled correlation. Possible application to multitone diffraction pattern sampling is also described. (13 min.)

\*Research supported in part by the Air Force Office of Scientific Research.

†California Institute of Technology, Pasadena, Calif. 91125.

This research has been considerably extended since the above report. However, the abstract above presents the status at the close of the subject contract. The later refinements will be described at the 1978 OSA Meeting in San Francisco, also under sponsorship by AFOSR; and they will be the subject of a paper in the JOSA.

## 2.2 Laser Propagation Through a Turbulent Gaseous Mixture (N. George and L. Pesselink)

A problem of particular interest in statistical optics is that of propagation through a random, time-varying atmosphere. For high speed aircraft using laser sensors, one would expect

† N. George and G.M. Morris, *J. Opt. Soc. Am.* 67, 1416 (1977).

to encounter both turbulences and shock waves. We seek to obtain a better understanding of this phenomenon. Recently, L. Hesselink, working with H. Liepmann and B. Sturtevant, designed and built a special chamber which, when added to the GALCIT shock tube, gives one the capability to produce controlled random atmospheres with fine scale turbulences of 1mm and a decay time of 100 ms.

While considerable experimentation had been performed with this apparatus using sound detectors and spark-gap light sources, N. George and L. Hesselink started a study of the effectiveness of laser light. Viewing the turbulent mixture as a cascaded diffuser, one would expect a strong wavelength dependence. In June-July of 1977, a series of experiments were performed using an argon laser operated first at a single wavelength and then multitone. Both motion pictures and single color photographs were obtained thereby demonstrating our hypothesis that multi-tone laser illumination is effective as an instrumentation technique for wind-tunnel experiments.

The status of this research at the close of effort under the subject contract is given by the following abstract of a talk presented at the annual meeting of the Optical Society of America in October 1977.<sup>†</sup>

TuL13. Laser Propagation Experiments Using A Controlled Turbulent Gaseous Mixture.\* NICHOLAS GEORGE, *The Institute of Optics, University of Rochester, Rochester, N. Y. 14627*, AND LAMBERTUS HESSELINK, *California Institute of Technology, Pasadena, Calif. 91125*. -In stellar speckle interferometry and many laser systems, the effect of atmospheric turbulence is a dominant issue. In prior work by one of us (LH), an apparatus has been constructed for generating a 25 cm cube of randomly inhomogeneous gas in the Guggenheim Aeronautical Laboratories 17-in.-diam. shock tube.<sup>1</sup> In the current study, we describe the use of this turbulent gas mixture to study laser propagation. Tunable lasers and multitone argon are useful either as a diagnostic for the gaseous mixture or as a means for studying speckle. In the chamber an array of fine jets in two opposing sidewalls is used to inject helium and freon-12 in a neutrally buoyant mixture. The optical index of refraction has an rms fluctuation as high as  $3 \times 10^{-6}$  with a turbulent microscale of 2 mm and an integral scale of 14 mm. High-speed motion pictures are shown of the Schlieren image of the turbulence and of the speckle image using transform plane stop and pinhole, respectively. A simulation of stellar speckle images of a point source or more complex input can be obtained by simple variations in the lens configuration. Preliminary analysis of the optical transfer function for this mixture are described in the context of our data using monochromatic, multitone, and white-light illumination. Some interesting color speckle patterns using "static" turbulence screens are also described and compared to the index inhomogeneities resulting in the test chamber. (13 min.)

\*Research supported in part by the Air Force Office of Scientific Research.

<sup>1</sup> L. Hesselink, "An Experimental Investigation of Propagation of Weak Shock Waves in a Random Medium." Ph.D. Thesis (California Institute of Technology, 1977).

### 2.3 Cumulative Listing of Publications on Speckle

Since 1972, the research in Speckle at the California Institute of Technology has been supported in part by the U.S. Air Force Office of Scientific Research. The following publications have resulted:

#### A. Subject Contract Period

"Randomly Serrated Edges, Lines and Apertures", J. Opt. Soc. Am. 67, 1416A<sup>++</sup> (1977), Nicholas George and G.M. Morris.

"Laser Propagation Experiments Using A Controlled Turbulent Gaseous Mixture", J. Opt. Soc. Am. 67, 1375A (1977), Nicholas George and Lambertus Hesselink.

+N. George and L. Hesselink, J. Opt. Soc. Am. 67, 1375 (1977).

++A following the page number means Abstract only.

## B. Prior AFOSR Contracts

"Speckle from rough moving objects", J. Opt. Soc. Am. 66, 1182 (1976), Nicholas George

"Speckle noise in displays", J. Opt. Soc. Am. 66, 1282 (1976), Nicholas George, C.R. Christensen, J.S. Bennett, B.D. Guenther.

"Topical issue on speckle", J. Opt. Soc. Am. 66, 1316 (1976), Nicholas George, Douglas C. Sinclair.

"Scattering by Glass Microballoons", J. Opt. Soc. Am. 66, 1135 A(1976), Nicholas George.

"Speckle Noise and Object Contrast", Symposium on Image Processing at Toronto, SPSE edit by R. Shaw (1976), B.D. Guenther, Nicholas George, C.R. Christensen, J.S. Bennett.

"Remote sensing of large roughened spheres", Optica Acta 23, 367 (1976), Nicholas George, A.C. Livanos, J.A. Roth, C.H. Papas.

"The Wavelength Sensitivity of Back-Scattering", Optics Communications 16, 328 (1976), Nicholas George.

"Speckle", Optics News 14, January 1976, Nicholas George.

"Speckle From a Cascade of Two Diffusers", Optics Communications 15, 71 (1975), Nicholas George and Atul Jain.

"Experiments on the Space and Wavelength Dependence of Speckle", Applied Physics - Invited Paper 7, 157 (1975), Nicholas George, Atul Jain, R.D.S. Melville.

"Spatial and Spectral Behavior of Speckle in an Imaging System", Ph.D. thesis Caltech 1975, Xerox Microfilm 75-20,003 by Richard D.S. Melville, Jr.

"Speckle, Diffusers, and Depolarization", Applied Physics 6, 65 (1975), Nicholas George, Atul Jain, R.D.S. Melville.

"A Wavelength Diversity Technique for Smoothing of Speckle", Ph.D. thesis Caltech 1974, Xerox Microfilm 74-XXXXXXX by Atul Jain.

"Space and Wavelength Dependence of Speckle Intensity", Applied Physics 4, 201 (1974), Nicholas George and Atul Jain.

"Speckle Reduction Using Multiple Tones of Illumination", Applied Optics 12, 1202 (1973), Nicholas George and Atul Jain, and abstract in J. Opt. Soc. Am. 62, 1356 A(1972).

"Speckle in Microscopy", Optics Communications 6, 253 (1972), Nicholas George and Atul Jain.

### 3. Photoresist Techniques for Integrated Optics

#### 3.1 Introduction

A really spectacular series of research accomplishments were obtained by a group (listed below) of scientists working on chirped-gratings as demultiplexers for dielectric waveguides. This topic of research was partially supported by the subject grant and partially supported by a separate grant from AFOSR with Professor Amnon Yariv as the Principal Investigator.

The portion of the research support drawn from the subject AFOSR contract included full support of Dr. Alexander C.R. Livanos as well as considerable laboratory facilitation for stabilized holography. Film supplies and other specialized electronics were also supported by funds from the subject contract. In this cooperative research, support for Dr. A. Katzir, one of the principal contributors, as well as that for Yariv, Hong, and Shellan was not derived from the subject contract. Appropriate accreditation to the U.S. Air Force Office of Scientific Research is contained in the resulting publications listed below in Sec. 3.2 and appended in their entirety in Sec. 3.3.

#### 3.2 Listing of Publications<sup>+</sup>

"Fabrication of Grating Structures with Variable Period", Optics Communications 20, 179 (1977), A.C. Livanos, A. Katzir, A. Yariv.

<sup>+</sup>Partially supported by the subject contract.

"Chirped-grating output couplers in dielectric waveguides", Applied Physics Letters 30, 225 (1977), A. Katzir, A.C. Livanos, A. Yariv.

"Chirped Gratings in Integrated Optics", IEEE J. Quantum Electronics QE-13, 296 (1977), A. Katzir, A.C. Livanos, J.B. Shellan, A. Yariv.

"Chirped-grating demultiplexers in dielectric waveguides", Applied Physics Letters 30, 519 (1977), A.C. Livanos, A. Katzir, A. Yariv, C.S. Hong.

"Linearity and enhanced sensitivity of the Shipley AZ-1350B photoresist", Applied Optics 16, 1633 (1977), A.C. Livanos, A. Katzir, J.B. Shellan, A. Yariv.

"Broad-band grating filters for thin-film optical waveguides", Applied Physics Letters 31, 276 (1977), C.S. Hong, J.B. Shellan, A.C. Livanos, A. Yariv, A. Katzir.

"Simultaneous exposure and development of photoresist materials: an analytical model", Applied Optics 16, 2612 (1977), P. Agmon, A.C. Livanos, A. Katzir, A. Yariv.

### 3.3 Appended Publications in Integrated Optics



width  $d$ , and the focus is located at point  $P(x_f, z_f)$ .

Simple geometrical considerations relate the focal line coordinates with  $f, s, d$ , and  $\theta$ , namely

$$z_f = \frac{1}{2}s \frac{\cos \theta + \cos(2\phi)}{\sin(2\phi)} \quad (1)$$

and

$$x_f = -z_f \tan(\frac{1}{2}\theta), \quad (2)$$

where

$$\phi = \tan^{-1}(\frac{1}{2}d/f)$$

is the convergence half angle.

The electric field on the film plate ( $z = 0$ ) is the sum of the reference wave and converging one and is given by

$$E(x, z = 0) = A \exp[-ikx \sin(\frac{1}{2}\theta)] + a \exp[ik\{(x - x_f)^2 + z_f^2\}^{1/2}], \quad (3)$$

where  $k = 2\pi/\lambda$  is the wave number for the incident fields,  $A$  and  $a$  the amplitudes of the plane and converging wave respectively. If we assume that the transmission function  $t$  of the hologram is proportional to  $EE^*$  [8], and that the amplitudes  $A$  and  $a$  are equal then:

$$t = \beta [1 + \cos\{kx \sin(\frac{1}{2}\theta) + k\sqrt{(x - x_f)^2 + z_f^2}\}], \quad (4)$$

where  $\beta$  is a proportionality constant. The period  $\Lambda$  for this particular grating is given by:

$$\Lambda(x) = \frac{\lambda}{\sin(\frac{1}{2}\theta) + (x - x_f)/\sqrt{(x - x_f)^2 + z_f^2}}. \quad (5)$$

In our experiment  $(x - x_f)^2 \ll z_f^2$  (paraxial case), therefore

$$\Lambda(x) = \frac{\lambda}{\sin(\frac{1}{2}\theta) + (x - x_f)/z_f}. \quad (6)$$

Furthermore, it can be shown that if the chirped grating is illuminated with a plane wave of wavelength  $\lambda'$  and angle of incidence (from the normal)  $\theta'$ , then the focal line (within the paraxial approximation) will shift to a new position  $P'$  with coordinates  $x'$  and  $z'$  given by [9]

$$z' = (\lambda/\lambda')z_f \quad (7)$$

and

180

$$x' = x_f + z' \sin \theta' - z_f \sin(\frac{1}{2}\theta). \quad (8)$$

To generate chirped gratings on photoresist the 4579 Å line of an argon laser was used to produce two collimated beams. The intensity of each beam was 3 mW/cm<sup>2</sup> and the angle between them was  $\theta = 26.5^\circ$ . A cylindrical lens of focal length  $f = 10$  cm, and width  $d = 2.4$  cm was inserted in one of the beams such that the interference pattern extended over a distance  $s = 0.65$  cm on the photoresist coated substrate. A neutral density wedge was introduced before the cylindrical lens so that the intensities of the plane and converging wave were identical on the film plane.

The fabrication of chirped gratings was demonstrated in a layer of Shipley AZ 1350J photoresist which was diluted 5:1 with thinner. The photoresist was spun coated at 6000 rpm on a well cleaned microscope slide, and then baked for 25 min at 90°C. Best results were obtained when this photoresist was exposed to the interference pattern for 125 sec (corresponding to 120 mJ/cm<sup>2</sup>), and then developed for 20 sec in AZ-303 developer [10].

Fig. 2 (continuous lines) shows the theoretical dependence of the period variation as a function of position and angle as given by eq. (6). The experimental points for  $\theta = 26.5^\circ$  were measured using a scanning electron microscope and the results (also shown on fig. 2) are in good agreement with theory.

In fig. 3 scanning electron microscope photographs

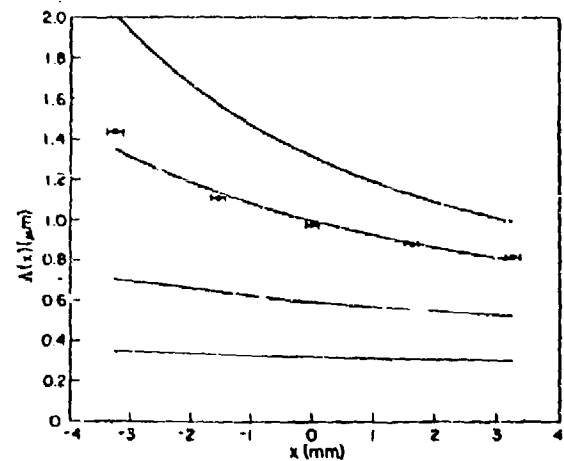
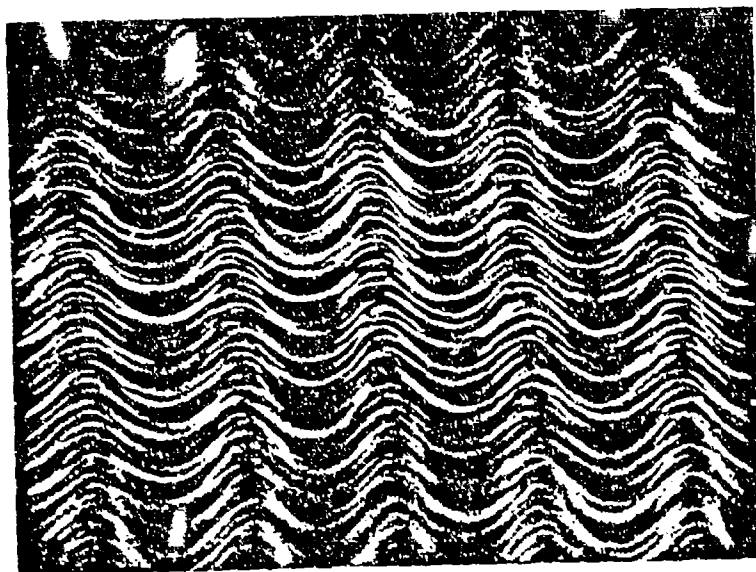
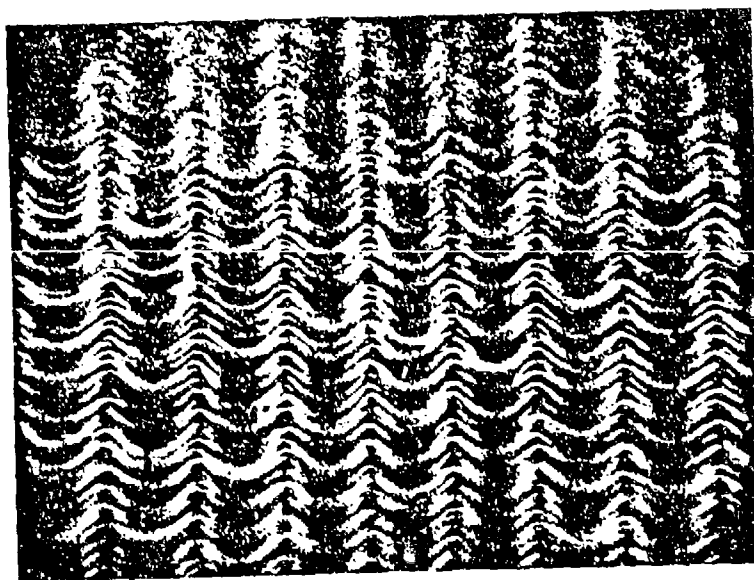


Fig. 2. Grating period ( $\Lambda$ ) variation as a function of position ( $x$ ) for various angles  $\theta$ . Experimental points for the case  $\theta = 26.5^\circ$  were obtained using a scanning electron microscope.



(a)



(b)

Fig. 3. Scanning electron microscope photographs of two regions of the chirped grating. (a) The grating at position  $x = -3.5$  mm corresponding to a period  $\Lambda(-3.5) = 1.43 \mu\text{m}$ . (b) The grating at  $x = 3.5$  mm with period  $\Lambda(3.5) = 0.82 \mu\text{m}$ .

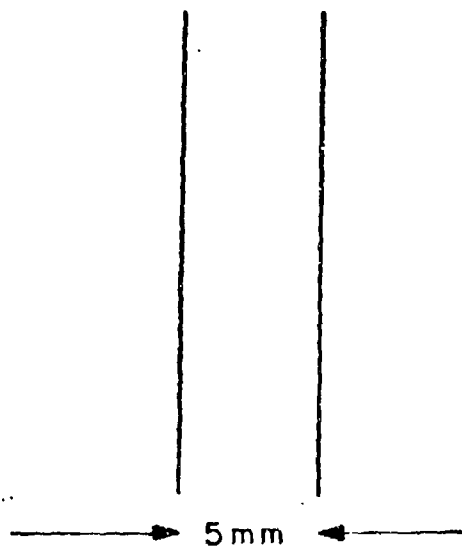


Fig. 4. Focal line separation obtained from simultaneous illumination of a chirped grating with 6328 Å and 5014 Å wavelengths.

of the grating period at  $x = -3.5$  mm [ $\Lambda(-3.5)$ ] and  $x = 3.5$  mm [ $\Lambda(3.5)$ ] are presented.

To illustrate the variation of the focus as a function of wavelength a chirped grating was illuminated simultaneously with collimating light from a He-Ne laser (6328 Å) and the green line (5014 Å) from an argon laser. Both beams passed through a spatial filter and a collimating lens, and were incident on the grating at an angle  $\theta = 0^\circ$ . A screen was positioned behind the

grating and the resulting focal lines, separated by a distance of 5 mm, are shown in fig. 4. The separation predicted by eq. (7) is 5.1 mm.

To summarize: The fabrication of chirped gratings in photoresist has been demonstrated and some of their properties studied. In addition, theoretical expressions describing the transmission function of these gratings have been presented [eq. (4)], as well as the periodicity as a function of lateral displacement [eq. (5)]. The variation of the focus as a function of wavelength and incident angle was also studied. The experimental results are in good agreement with the theory.

An experiment which involves the use of a chirped grating in optical multiplexing is now in progress.

#### References

- [1] H.L. Garvin, E. Garmire, S. Somekh, H. Stoll and A. Yariv, *Appl. Opt.* 12 (1973) 455.
- [2] H.L. Dakss, L. Kuhn, P.F. Heidrich and B.A. Scott, *Appl. Phys. Lett.* 16 (1970) 523.
- [3] J.J. Clair, J.M.C. Jonathan and J.L. Stehle, *Opt. Commun.* 13 (1975) 183.
- [4] M. Nakamura, H.W. Yen, A. Yariv, E. Garmire, S. Somekh and H.L. Garvin, *Appl. Phys. Lett.* 23 (1973) 224.
- [5] D.C. Flanders, H. Kogelnik, R.V. Schmidt and C.V. Shank, *Appl. Phys. Lett.* 24 (1974) 194.
- [6] H. Stoll, A. Yariv, *Opt. Commun.* 8 (1973) 5.
- [7] G. Rogers, *Nature* 166 (1950) 273.
- [8] R.A. Bartolini, *Appl. Opt.* 13 (1974) 129.
- [9] J.W. Goodman, *Introduction to Fourier Optics* (McGraw Hill, San Francisco, 1968), 214.
- [10] S.L. Norman and M.P. Singh, *Appl. Opt.* 14 (1975) 818.

# Chirped-grating output couplers in dielectric waveguides\*

A. Katzir, A. C. Livanos, and A. Yariv

California Institute of Technology, Pasadena, California 91125  
(Received 4 August 1976, in final form 29 November 1976)

This paper reports on the method of fabrication and first experiments of chirped (variable period) gratings in a dielectric waveguide. Such gratings, which are proposed as a new optical building block, are used in this work as focusing output couplers.

PACS numbers: 84.40.Wv, 42.80.Lt, 42.82.+n, 42.80.Fn

Periodic perturbations such as surface corrugations are often used for input or output couplers in dielectric waveguides.<sup>1</sup> A guided optical mode can be coupled out by surface gratings at an angle  $\phi$  with respect to the film surface, where  $\phi$  is determined by the propagation constant  $\beta$  of light in the waveguide and by the period  $\Lambda$ . If the output coupler consists of a grating with a variable period  $\Lambda(x)$ , then, for a given propagating mode, different parts of the coupler would launch the light out in different directions. It is conceivable that all these directions will intersect at a common point in such a way that the light will be focused outside the waveguide.

To ensure this type of focusing we fabricated the grating holographically by exposing a photoresist layer on top of the waveguide to the interference of a collimated laser beam and a cylindrically focused beam. The photoresist grating which remained after development served as a mask through which the grating was replicated, by ion etching, onto the waveguide surface. Similar exposure schemes have been used for the fabrication of holographic lenses.<sup>2</sup>

The setup used for the fabrication of chirped gratings is shown schematically in Fig. 1. A thin layer of recording material is exposed to the interference pattern of a collimated laser beam with a converging beam. The converging beam is generated by a cylindrical lens of focal length  $f$  and width  $d$ . The bisector of this beam subtends an angle  $\theta$  with the collimated beam. The coordinates  $x_f$  and  $z_f$  of the focal point  $P$  are simple geometrical functions of  $f$ ,  $d$ ,  $\theta$ , and  $L$ , where  $L$  is the

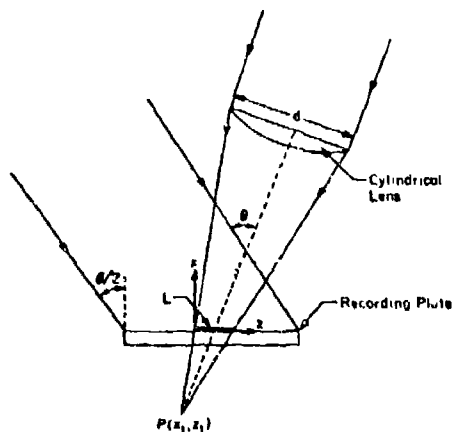


FIG. 1. Recording arrangement and geometry for the fabrication of chirped gratings.

length of the recorded pattern (see Fig. 1). One can assume that the transmission function  $t$  of the recording medium is proportional to  $EE^*$  and derive the following expression for  $t$ :

$$t = \beta \{ 1 + \cos \{ kx \sin(\frac{1}{2}\theta) + k[(x - x_f)^2 + z_f^2]^{1/2} \} \}, \quad (1)$$

where  $\beta$  is a proportionality factor. The period  $\Lambda(x)$  can now be written

$$\Lambda(x) = \frac{\lambda}{\sin(\frac{1}{2}\theta) + (x - x_f) [(x - x_f)^2 + z_f^2]^{-1/2}}. \quad (2)$$

The period is therefore a function of  $\lambda$ ,  $\theta$ ,  $f$ ,  $d$ , and  $L$ . Each of these can be changed, independently, so as to give a different variation  $\Lambda(x)$ .

The interference pattern described above was used, as discussed above, to fabricate chirped gratings on top of sputtered glass waveguides.

Consider next the dielectric waveguide shown schematically in Fig. 2. The surface of the waveguide is corrugated over a length  $L$ , and the corrugation period is given by Eq. (2). For a given propagating mode with a propagation constant  $\beta = kn_1 \cos\theta_1$ , the light coupled out at a point  $x'$  along the grating will propagate in air according to

$$\exp(i\{k_x(x')z + [(\omega/c)^2 - k_x^2(x')]z^2\}^{1/2}),$$

where  $k_x(x') = \beta - 2\pi/\Lambda(x')$ . If we define  $\beta_0 = k_x(0) = \beta - 2\pi/\Lambda(0)$  and  $\beta_L = k_x(L) = \beta - 2\pi/\Lambda(L)$ , it can now be shown that the light will be focused by the chirped grating at a point  $P(x_2, z_2)$  whose coordinates are given by

$$z_2 = \frac{\beta_0 L (k^2 - \beta_L^2)^{1/2}}{\beta_0 (k^2 - \beta_L^2)^{1/2} - \beta_L (k^2 - \beta_0^2)^{1/2}}, \quad (3)$$

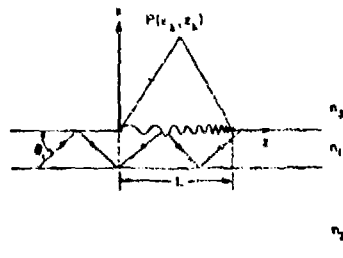


FIG. 2. Geometry for a chirped grating etched on the top surface of a waveguide of index  $n_1$ . The substrate has an index  $n_2$ , and  $n_3$  is the index of refraction of air. A waveguide mode will focus at point  $P(x_2, z_2)$  depending on the waveguide, the chirp of the grating, and the wavelength.

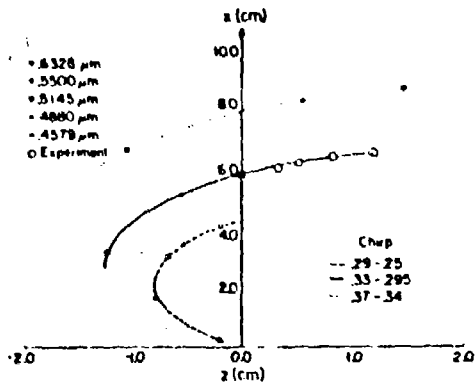


FIG. 3. Experimental and theoretical results of the focusing of light for the corrugated structure used. The solid line represents the theoretical position of the focus as a function of wavelength. The solid dots represent the focus of the prominent lines of the Ar<sup>+</sup> and HeNe lasers. The large circles are the experimental points for these wavelengths as measured with a two-dimensional translation probe.

$$x_\lambda = [(k^2 - \beta_0^2)^{1/2} / \beta_0] z_\lambda. \quad (4)$$

The focal-point coordinates thus depend on the chirp of the gratings, on the waveguide, and on the wavelength of the guided mode. Some examples of the variation of the focal point with wavelength and with chirping are given (for a particular waveguide) in Fig. 3.

To illustrate the focusing effect we designed a waveguide to focus light a few centimeters away from the waveguide. We first used ion sputtering to deposit a layer of 7059 glass on a regular microscope slide. The refractive index of the waveguide was determined by the prism coupler method<sup>4</sup> and was found to be 1.565. The thickness of the deposited layer was determined by Sloan Dektak. The thickness was 1.35  $\mu\text{m}$  and was found to be uniform within 5% over the region of interest. A thin layer of undiluted AZ-1350B Shipley photoresist was then spin coated on the waveguiding layer at 3600 rpm. The photoresist was prebaked at 125°C for 25 min and then exposed to the interference pattern between the collimated beam and the converging beam. In this experiment we used the  $\lambda = 4579 \text{ \AA}$  line of an Ar<sup>+</sup> laser, with 1.0 mW/cm<sup>2</sup> per leg. The other variables were  $\theta = 94.5^\circ$ ,  $F = 1.33$ , and  $L = 1.1 \text{ cm}$ . The photoresist layer was exposed for 60 sec, and then developed for 10 sec in AZ-303A developer. Chirped gratings were thus obtained and the grating period was measured and found to vary between  $\Lambda(0) = 0.295 \text{ \mu m}$  and  $\Lambda(z = 1.1 \text{ cm}) = 0.33 \text{ \mu m}$ . The photoresist was then baked in vacuum, and the chirped grat-

ings were transferred onto the waveguide using the same ion beam etching machine.

We calculated the position of the focal point  $P(x_\lambda, z_\lambda)$  for various lines of the Ar<sup>+</sup> laser. For each line, and for the waveguide used, we calculated the propagation constant and obtained  $x_\lambda$  and  $z_\lambda$ . The results of these calculations are shown in Fig. 3, both for the chirped gratings used and for other chirped gratings.

In the experiment we used a prism coupler to couple light from an Ar<sup>+</sup> laser into the waveguide. The light coupled by the grating was found to focus to a line normal to the  $xz$  plane. The  $x$ - $z$  coordinates of this line were measured for various lines of an Ar<sup>+</sup> laser. The experimental points are also shown in Fig. 3, and are found to fit well to the theoretical curve. It should be noted that the focal point moves 1.2 cm when the wavelength is changed from 4579 to 5145  $\text{\AA}$ .

In conclusion we demonstrated in this work the fabrication of a chirped-grating output coupler in an optical waveguide. This structure focuses light outside the waveguide while simultaneously separating between propagating beams of different wavelengths.

Various integrated optics components are based on a periodic perturbation. Such components as narrow-band reflection filters,<sup>5</sup> beam splitters,<sup>6</sup> distributed feedback lasers,<sup>7</sup> distributed Bragg reflectors,<sup>8</sup> and grating couplers<sup>9</sup> are all based on a periodic perturbation. Very often the perturbation takes place as a surface corrugation. The addition of a new variable, chirping, into these components is bound to open up new possibilities in their utilization.

The authors wish to thank Professor N. George for many helpful discussions and D. R. Armstrong for his assistance.

\*Research supported by Air Force Office of Scientific Research.

<sup>1</sup>M. L. Dakss, L. Kuha, P. F. Heidrich, and B. A. Scott, *Appl. Phys. Lett.* **16**, 523 (1970).

<sup>2</sup>G. Rogers, *Nature* **166**, 273 (1950).

<sup>3</sup>R. A. Bartolini, *Appl. Opt.* **13**, 129 (1974).

<sup>4</sup>R. Ulrich and K. Torge, *Appl. Opt.* **12**, 2901 (1973).

<sup>5</sup>D. C. Flanders, H. Kogelnik, R. V. Schmidt, and C. V. Shank, *Appl. Phys. Lett.* **24**, 194 (1974).

<sup>6</sup>K. S. Pennington and L. Kuhn, *Opt. Comm.* **3**, 387 (1971).

<sup>7</sup>K. Aiki, M. Nakamura, J. Umeda, A. Yariv, A. Katzir, and H. W. Yen, *Appl. Phys. Lett.* **27**, 145 (1975).

<sup>8</sup>W. Ng, H. W. Yen, A. Katzir, I. Samid, and A. Yariv, *Appl. Phys. Lett.* **30**, 684 (1976).

# Chirped Gratings in Integrated Optics

A. KATZIR, A. C. LIVANOS, J. B. SHELLAN, AND A. YARIV

**Abstract**—Gratings with variable periods (chirped gratings) have been fabricated by recording the interference pattern of a collimated laser beam with a converging beam generated by a cylindrical lens. An analysis is presented for the behavior of the chirped gratings as a function of wavelength, the angle between the illuminating beams, the  $F$  number of the lens, and its position. To calculate the power radiated into air, the coupled-mode equations are solved for the case of a waveguide with chirped surface corrugation. Experimentally, chirped gratings have been etched on the surface of an optical waveguide and used to couple light out of the waveguide. It was found that the light was focused outside the waveguide, and the fraction of the power radiated into air compared favorably with the theoretical calculation. The focal point outside the waveguide was found to move by about 1 cm when the wavelength was changed by 500 Å—in agreement with theoretical estimates.

## I. INTRODUCTION

**P**ERIODIC STRUCTURES, and in particular corrugated structures, play a significant role in integrated optics [1]. Corrugated waveguides serve as narrow-band filters, which reflect wavelengths which satisfy Bragg's law [2]. Such reflectors may be incorporated in laser structures to form distributed feedback lasers [3] or distributed Bragg reflectors [4]. Periodic structures with longer periods have been used to couple between guided modes and air, such as in the cases of input or output couplers [5].

In this paper, we consider the problem of gratings with large and monotonic variation in the period. We describe a method for fabricating such chirped gratings, present a theory for treating them, and present experimental results demonstrating some of their unique applications.

## II. GRATING FABRICATION CONSIDERATIONS

The gratings are fabricated, as in the case of uniform gratings, by the interference of two laser beams. The period chirp is obtained by cylindrical focusing of one of the two beams, as shown in Fig. 1. The recording plate is located at the  $x = 0$  plane, the angle of incidence of the plane wave is  $\theta/2$ , and the angle subtended by the collimated beam and the bisector of the converging beam angle is  $\theta$ . The interference pattern is recorded over a distance  $L$  on the recording plate. The converging wave is generated by a cylindrical lens of focal length  $f$  and width  $d$ , and the focus is located at point  $P(x_f, z_f)$ .

Simple geometrical calculations relate the focal line coordinates with  $f, L, d$ , and  $\theta$ , namely

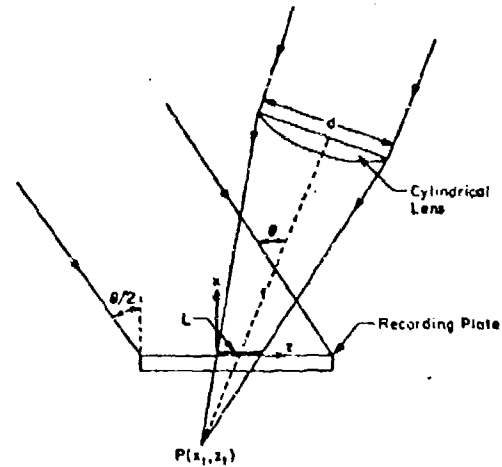


Fig. 1. Recording arrangement and geometry for the fabrication of chirped gratings.

$$x_f = \frac{-L \cos\left(\phi + \frac{\theta}{2}\right)}{2 \sin 2\phi} \cos\left(\phi - \frac{\theta}{2}\right) \quad (1)$$

and

$$z_f = \frac{L \cos\left(\phi + \frac{\theta}{2}\right)}{\sin 2\phi} \sin\left(\phi - \frac{\theta}{2}\right) \quad (2)$$

where

$$\phi = \tan^{-1}\left(\frac{d}{2f}\right)$$

is the convergence half-angle. We note that in (1)  $x_f$  is always negative, while  $z_f$  can take negative or positive values depending on the angles  $\theta$  and  $\phi$ .

The electric field in the recording plane ( $x = 0$ ) is given by the sum of the reference wave and converging one and is given by

$$E(x=0, z) = A \exp - ikz \sin(\theta/2) + \alpha \exp ik \left\{ [(x - z_f)^2 + z_f^2]^{1/2} \right\} \quad (3)$$

where  $k = 2\pi/\lambda$  is the wavenumber for the incident field, and  $A$  and  $\alpha$  are the amplitudes of the plane and converging wave, respectively. If we assume that the transmission function of the recording medium  $t$  is proportional to  $EE^*$  [6], and that  $A = \alpha$ , then

$$t = \beta \left\{ 1 + \cos \left[ kz \sin(\theta/2) + k \sqrt{(x - z_f)^2 + z_f^2} \right] \right\} \quad (4)$$

where  $\beta$  is a proportionality constant. The period  $\Lambda$  for this particular grating is given by

Manuscript received November 16, 1976; revised December 16, 1976. This research was supported by AFOSR. The work of one of the authors (J. B. S.) was supported in part by the Hertz Foundation.

The authors are with the California Institute of Technology, Pasadena, CA 91125.

$$\Lambda(z) = \frac{\lambda}{\sin(\theta/2) + \frac{z - z_f}{\sqrt{(z - z_f)^2 + x_f^2}}} \quad (5)$$

In the paraxial approximation  $(z - z_f)^2 \ll x_f^2$ , (4) and (5) reduce to

$$t = \beta \left[ 1 + \cos \left\{ \frac{k}{2x_f} z^2 + \left( k \sin(\theta/2) - \frac{kz_f}{x_f} \right) z + kx_f + \frac{kz_f^2}{2x_f} \right\} \right] \quad (6)$$

The corresponding expression for (5) is therefore

$$\Lambda(z) = \frac{\lambda}{\sin(\theta/2) + (z - z_f)/x_f} \quad (7)$$

It is seen from (1), (2), and (5) that the period variation  $\Lambda(z)$  depends on the  $F$  number of the lens ( $F \equiv f/d$ ), and that  $\theta$  is the angle subtended by the collimated beam and the bisector of the converging beam angle,  $\lambda$  is the wavelength of illumination, and  $L$  is the length of the grating.

The dependence of the period variation on  $F$  is illustrated by Figs. 2 and 3. In Fig. 2, the angle  $\theta$  is set at  $60^\circ$  and the grating has a total length of 1 cm. For various  $F$  numbers, period variations from  $0.8 \mu\text{m}$  to  $0.4 \mu\text{m}$  are obtained. The lower the  $F$  number the greater the period variation; higher  $F$  numbers result in smaller and more linear period variations. In Fig. 3, the angle  $\theta$  has the value of  $90^\circ$ . Here the maximum period variation is for an  $F = 1$  lens and it extends from  $0.45$  to  $0.28 \mu\text{m}$  over a distance of 1 cm. It is noted that large values of  $\theta$  produce smaller period variations.

This particular point is illustrated in Fig. 4, where an  $F = 1.33$  lens was chosen and  $\theta$  was varied from  $45^\circ$  to  $120^\circ$ . Again the grating extends over a distance of 1 cm. It is seen that with  $\theta = 120^\circ$ , the period varies only by  $0.05 \mu\text{m}$ , while for  $\theta = 45^\circ$  the period variation is  $0.5 \mu\text{m}$ .

The linearity of the period variation as a function of grating length  $L$  is shown in Fig. 5. It should be noted that the beginning and end period is identical for all values of  $L$ . Again the  $F$  number is 1.33 and the angle  $\theta$  is  $90^\circ$ .

### III. WAVEGUIDE COUPLING

Chirped grating etched onto a dielectric waveguide results in a simultaneous output coupling and focusing to a point  $P(z_\lambda, z_\lambda)$ , which will vary as a function of the modes supported by the waveguide and the wavelength of the guided modes.

Consider the geometry described by Fig. 6. When the guided mode is propagating unperturbed in the waveguide, its  $z$  dependence is given by  $e^{-i\beta z}$ , where  $\beta = kn_z \cos \theta_z$ . When the wave reaches the perturbation, the radiated mode will have a  $z$  dependence given by  $e^{-ik_x z}$ . At point  $z = 0$ ,  $k_x$  is given by

$$k_x(0) = \beta - \frac{2\pi}{\Lambda(0)} \quad (8)$$

and at  $z = L$

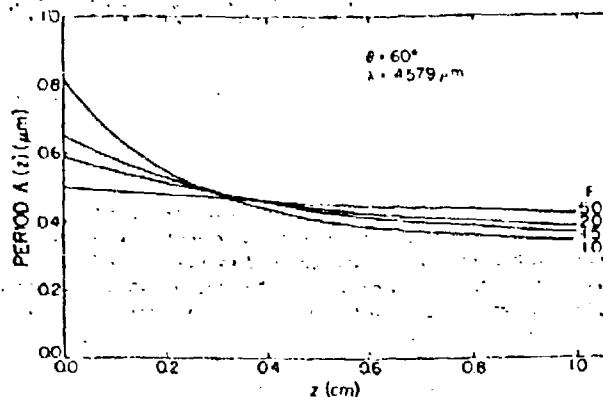


Fig. 2. Period variation as a function of the  $F$  number of the converging lens ( $F = f/d$ ). The angle  $\theta = 60^\circ$  is suitable for variations of  $0.8$ – $0.4 \mu\text{m}$  over a distance of 1 cm.

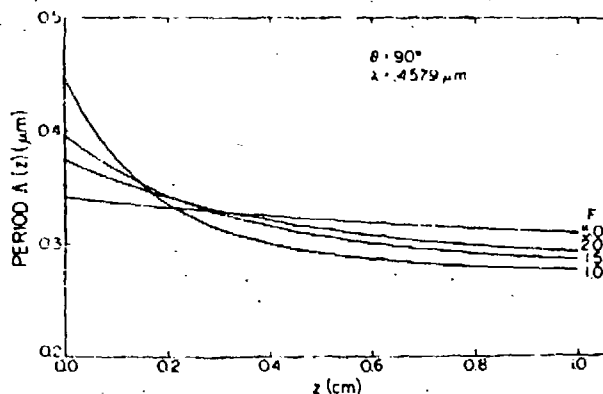


Fig. 3. Period variation as a function of the  $F$  number. The angle  $\theta$  has a value of  $90^\circ$  and the range of period variation is from  $0.45$  to  $0.28 \mu\text{m}$ , again over a distance of 1 cm.

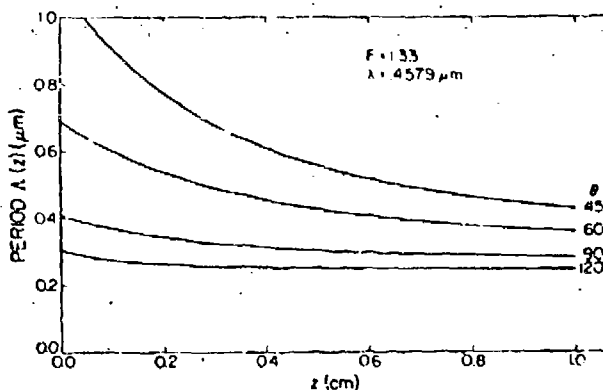


Fig. 4. Period variation as a function of  $\theta$  (the angle between the plane wave and the bisector of the converging wave). The  $F$  number of the lens is 1.33 and the illumination wavelength is  $0.4579 \mu\text{m}$ . The recording distance is kept constant at 1 cm.

$$k_x(L) = \beta - \frac{2\pi}{\Lambda(L)} \quad (9)$$

It can be shown that by a) matching the tangential component of the electric field inside and outside the waveguide, b) requiring that  $k^2 = k_z^2 + k_x^2$  outside the waveguide, and c)

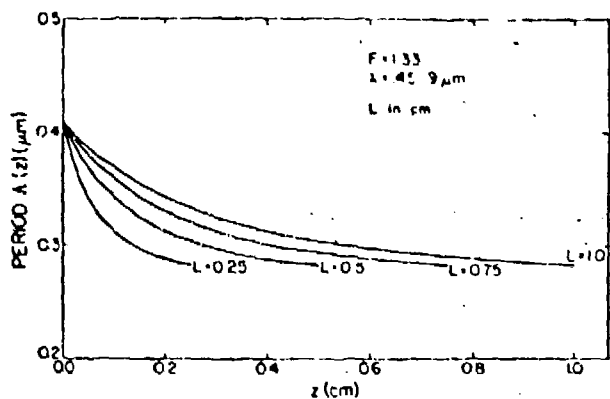


Fig. 5. Period variation as a function of recording distance  $L$ . The total amount of chirp is the same for all curves; the linearity of variation is seen to improve for large values of  $L$ . The angle  $\theta$  is  $50^\circ$ , the  $F$  number is 1.33, and the wavelength is  $0.4579 \mu\text{m}$ .

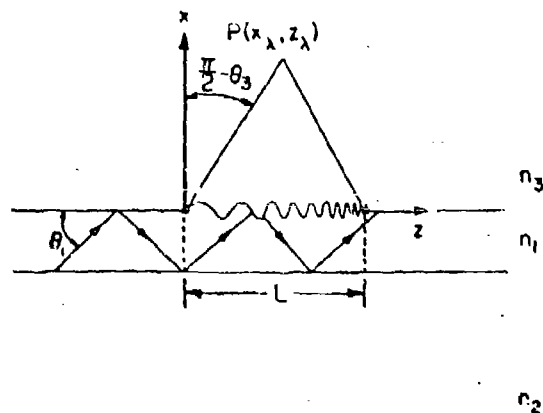


Fig. 6. Geometry for a chirped grating etched on the top surface of a waveguide of index  $n_1$ . The substrate has an index  $n_2$ , and  $n_3$  is the index of refraction of air. A waveguide mode will focus at point  $P(x_\lambda, z_\lambda)$ , depending on the chirp of the grating and the wavelength.

assuming that the transmission function for the grating is given by (4), the light will focus outside at a point  $P(x_\lambda, z_\lambda)$  given by

$$z_\lambda = \frac{k_x(0)L\sqrt{k^2 - k_z^2(L)}}{k_x(0)\sqrt{k^2 - k_z^2(L)} - k_x(L)\sqrt{k^2 - k_z^2(0)}} \quad (10)$$

and

$$x_\lambda = \frac{\sqrt{k^2 - k_z^2(0)}}{k_x(0)} z_\lambda \quad (11)$$

The focusing effect and especially the variation of the focus as function of wavelength and period variation is illustrated by Fig. 7. Taking  $n_1 = 1.565$ ,  $n_2 = 1.51$ ,  $n_3 = 1.0$ , and a waveguide thickness of  $d = 1.35 \mu\text{m}$ , the eigenvalue equation for  $\beta$  was solved for wavelengths ranging from 4500 to 6500 Å. Having thus determined  $\beta$  for the unperturbed waveguide, we calculate  $k_x(0)$ ,  $k_x(L)$  for various ranges of period variation. It can be seen from this figure that a) the larger the period variation the closer to the waveguide the locus of the focal points will be, b) the smaller the period variation the larger

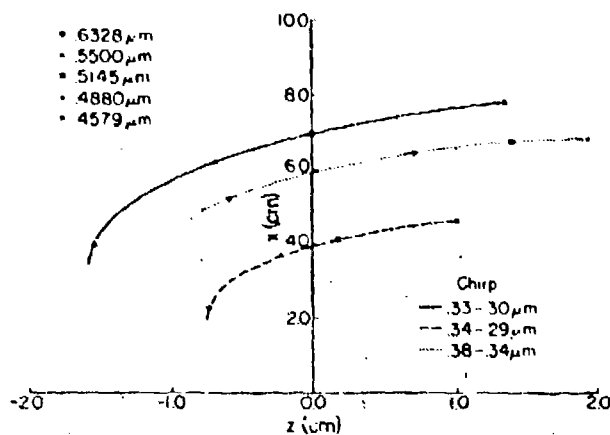


Fig. 7. Locus of the focal of various wavelengths for different chirps. The grating is located between  $z = 0$  and  $z = 1.0 \text{ cm}$  at  $x = 0$ .  $\Lambda(0)$  is the longest period and  $\Lambda(1 \text{ cm})$  is the shortest. The waveguide mode is traveling in the positive  $z$  direction.

the separation between the different wavelengths and the larger the distance of the locus of the focal points from the waveguide, and c) if the average period of the chirped grating is increased the focus will shift towards greater values of  $z$ .

#### IV. CALCULATION OF POWER OUTPUT DISTRIBUTION FOR CHIRPED GRATINGS

In the previous section we discussed the characteristics of the chirped gratings and some of their properties. To complete our theoretical discussion we present a calculation of the actual power radiated into air by a chirped grating.

To analyze this problem we expand the electric field of the perturbed waveguide in terms of the guided modes, the substrate modes, and the air modes. This work is essentially an extension of Marcuse's work [7], in so much that in our case the waveguide is no longer symmetric (we include the substrate). Our notation and method are similar to his.

We present a closed-form solution for the power radiated into air by a chirped grating, and illustrate the solution with examples of gratings where we vary the amount of chirp and the wavelength of the guided radiation.

Consider the geometry and notation as presented in Fig. 8(a). Using the results obtained by Marcuse [8], we have for the TE guided modes

$$\delta_y = A e^{-\delta x}, \quad \text{for } x > 0 \quad (12)$$

$$= A \left[ \cos \kappa x - \frac{\delta}{\kappa} \sin \kappa x \right], \quad \text{for } 0 > x > -d \quad (13)$$

$$= A \left[ \cos \kappa d + \frac{\delta}{\kappa} \sin \kappa d \right] e^{\gamma(x+d)}, \quad \text{for } x < -d \quad (14)$$

where

$$\kappa \equiv (n_1^2 k^2 - \beta^2)^{1/2} \quad (15)$$

$$\gamma \equiv (\beta^2 - n_2^2 k^2)^{1/2} \quad (16)$$

$$\delta \equiv (\beta^2 - n_3^2 k^2)^{1/2} \quad (17)$$

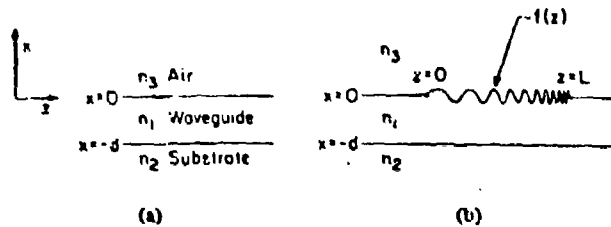


Fig. 8. (a) Geometry for a dielectric waveguide. (b) Dielectric waveguide with a chirped grating etched on the top surface.

where  $n_1$ ,  $n_2$ ,  $n_3$  are the indices of refraction of the waveguide, substrate, and air, respectively,  $k$  is the wavenumber in air, and  $\beta$  describes the  $z$  dependence of the electric field. It should be noted that the factor  $e^{i\omega t} e^{-i\beta z}$  has been suppressed in (12)-(14). Furthermore, the constants  $\kappa$ ,  $\gamma$ , and  $\delta$  can be determined by the eigenvalue equation

$$\tan \kappa d = \frac{\kappa(\gamma + d)}{\kappa^2 - \gamma\delta} \quad (18)$$

The amplitude of the electric field  $A$  is related to the power carried by the mode, namely

$$A^2 = \frac{4\kappa^2 \omega \mu_0 P}{|\beta| [d + 1/\gamma + 1/\delta] (\kappa^2 + \delta^2)} \quad (19)$$

$$P = \frac{\beta}{2\omega \mu_0} \int_{-\infty}^{\infty} |\delta_y|^2 dx$$

where  $P$  is the power carried by the mode,  $d$  is the thickness of the guide,  $\omega$  is the radian frequency, and  $\mu_0$  is the magnetic permeability of vacuum.

These guided modes occur for  $\kappa n_2 < |\beta| < \kappa n_1$ . For the region  $\kappa n_2 < |\beta| < \kappa n_1$  the substrate modes exist, and, finally, in the region  $0 < |\beta| < \kappa n_3$  the TE air modes of the continuum occur. For the purposes of this discussion we consider the air mode since we want to calculate the power radiated by the waveguide into the air. Reference [8] gives the electric field as

$$\delta_y^a = C_r [\cos \Delta x + (\sigma/\Delta) F_1 \sin \Delta x] \quad \text{for } x \geq 0 \quad (20)$$

$$= C_r (\cos \sigma x + F_1 \sin \sigma x) \quad \text{for } 0 \geq x \geq -d \quad (21)$$

$$= C_r [(\cos \sigma d - F_1 \sin \sigma d) \cos \rho(x+d) + \frac{\sigma}{\rho} (\sin \sigma d + F_1 \cos \sigma d) \sin \rho(x+d)], \quad \text{for } x < -d \quad (22)$$

$$\Delta = (n_3^2 k^2 - \beta^2)^{1/2} \quad (23)$$

$$\sigma = (n_1^2 k^2 - \beta^2)^{1/2} \quad (24)$$

$$\rho = (n_2^2 k^2 - \beta^2)^{1/2} \quad (25)$$

where  $C_r$  is again related to the power carried by the mode

$$C_r^2 = \frac{4\omega \mu_0 P}{\pi |\beta|} [(\cos \sigma d - F_1 \sin \sigma d)^2$$

$$+ \frac{\sigma^2}{\rho^2} (\sin \sigma d + F_1 \cos \sigma d)^2 + \left(1 + \frac{\sigma^2}{\Delta^2} F_1^2\right) \left(\frac{\Delta}{\rho}\right)^{-1}]^{-1} \quad (26)$$

and  $F_1$  can be chosen arbitrarily. Following the conventional procedure,  $F_1$  and  $F_2$  are chosen so that the two radiation modes are orthogonal to one another.

$$F_{1,2} = [(\sigma^2 - \rho^2) \sin 2\sigma d]^{-1} \left\{ (\sigma^2 - \rho^2) \cos 2\sigma d + \left(\frac{\rho}{\Delta}\right) (\sigma^2 - \Delta^2) \pm [(\sigma^2 - \rho^2)^2 + 2(\rho/\Delta)(\sigma^2 - \rho^2)(\sigma^2 - \Delta^2) \cdot \cos 2\sigma d + (\rho^2/\Delta^2)(\sigma^2 - \Delta^2)^2]^{1/2} \right\} \quad (27)$$

where

$$P\delta(\rho - \rho') = \frac{\beta^2}{2\omega \mu_0} \int_{-\infty}^{\infty} \delta_y^a(\rho) \delta_y^{a*}(\rho') dx.$$

Again the factor  $e^{i\omega t} e^{-i\beta z}$  has been suppressed in (20)-(22). In this work  $\beta$  is an inherently positive quantity.

Next we expand an arbitrary TE electric field for the perturbed waveguide in terms of the discrete guided modes and the continuum of both substrate and air modes

$$E_y = \sum_{\text{discrete}} C_n(z) \delta_n + \int_0^{(n_1^2 - n_2^2)^{1/2}} g(\rho, z) \delta^s(\rho) d\rho + \sum_{\substack{\text{even} \\ \text{odd}}} \int_{\kappa(n_1^2 - n_2^2)}^{\kappa n_3} h(\rho, z) \delta^a(\rho) d\rho \quad (28)$$

where  $\delta_n$  are the discrete guided modes given by (12)-(14) for the  $n$  values of  $\beta$  determined from the eigenvalues of (18). Similarly,  $\delta^a$  are the air modes given again by (20)-(22), where even and odd refer to the choice of  $F_2$  and  $F_1$  (27).  $\delta^s$  are the substrate modes which have not been presented explicitly since they do not affect this calculation. It is to be noted that the previous expansion for the total electric field  $E_y$  is possible since the set of eigenfunctions is complete. The calculation is simplified due to the orthogonality of the modes as a result of the choice of  $F_j$ . Furthermore, this expansion is similar to the one present in [7], as well as the notation and the method used to solve this problem.

To determine the value of  $h(\rho, z)$ , we substitute (28) into the Helmholtz wave equation, multiply by  $\delta^{a*}$ , integrate over  $x$ , and, using the orthogonality relations, get a differential equation for  $h(\rho, z)$ . This differential equation is then converted into an integral equation following the procedures of [7], namely

$$h(\rho, z) = Q(\rho) + R(\rho) \exp 2i\beta z + \frac{1}{2i\beta} \int_0^z [\exp 2i\beta(x-\xi) - 1] H(\rho, \xi) d\xi \quad (29)$$

where

$$\begin{aligned}
 H(\rho, z) = & \frac{-\beta k^2}{2\omega\mu P} \left[ \sum_n C_n(z) \int_{-\infty}^{\infty} \mathcal{E}^{**}(\rho) \Delta n^2 \mathcal{E}_n dx \right. \\
 & + \int_{k(n_1^2 - n_2^2)^{1/2}}^{kn_1} d\rho' g(\rho', z) \int_{-\infty}^{\infty} \mathcal{E}^{**}(\rho) \\
 & \cdot \Delta n^2 \mathcal{E}^*(\rho') dx + \int_{k(n_1^2 - n_2^2)^{1/2}}^{kn_1} d\rho' h(\rho', z) \\
 & \cdot \int_{-\infty}^{\infty} \mathcal{E}^{**}(\rho) \Delta n^2 \mathcal{E}^*(\rho') dx \quad (30)
 \end{aligned}$$

where  $\Delta n^2$  describes the deviation of the corrugated-guide dielectric constant from that of a uniform waveguide.

To solve the previous integral equation, we use the Born approximation. In other words, we use  $C_n(0) = \delta_{0n}$  instead of  $C_n(z)$  and set  $g(\rho, z) = h(\rho, z) = 0$ , in (30), resulting in

$$H(\rho, z) \approx \frac{-\beta k^2}{2\omega\mu P} \int_{-\infty}^{\infty} \mathcal{E}^{**}(\rho) \Delta n^2 \mathcal{E}_0 dx. \quad (31)$$

In the next step, we assume that the perturbation of the guide from its ideal shape is on the top surface of the guide, as shown in Fig. 8(b). By taking a shallow grating and setting  $x = 0$  in the previous equation, we get

$$H(\rho, z) = \frac{-\beta k^2}{2\omega\mu P} (n_1^2 - n_2^2) f(z) \mathcal{E}^{**}(0, \rho, z) \mathcal{E}_0(0, z). \quad (32)$$

Equation (29) can then be divided into parts as follows:

$$h^+ = Q - \frac{1}{2i\beta} \int_0^z H(\rho, \xi) d\xi \quad (33)$$

$$h^- = \left[ R + \frac{1}{2i\beta} \int_0^z \exp(-2i\beta\xi) H(\rho, \xi) d\xi \right] \exp(2i\beta z) \quad (34)$$

such that

$$h = h^+ + h^-.$$

Recalling (28), we note that the contribution to the total electric field arises from the product of  $h(\rho, z) \cdot \mathcal{E}^*(\rho, z)$ . The  $z$  dependence of  $\mathcal{E}^*(\rho, z)$  is  $e^{-i\beta z}$ . If we consider the  $z$  dependence of the product, then

$$\begin{aligned}
 h(\rho, z) \mathcal{E}^*(\rho, z) = & h^+ \exp(-i\beta z) + \left[ R + \frac{1}{2i\beta} \right. \\
 & \left. \int_0^z \exp(-2i\beta\xi) H(\rho, \xi) d\xi \right] \exp(i\beta z). \quad (35)
 \end{aligned}$$

Then we can associate the  $h^+$  part of the wave with the amplitude of the forward-traveling radiating mode and the term in brackets with the negative-traveling one.

The power radiated into air is given by

$$\begin{aligned}
 \left( \frac{\Delta P}{P} \right)_{\text{radiated into air}} = & \sum_{\substack{\text{even} \\ \text{odd}}} \int_{k(n_1^2 - n_2^2)^{1/2}}^{kn_1} d\rho \left\{ |h^+(\rho, L)|^2 \right. \\
 & \left. + |h^-(\rho, 0)|^2 \right\} \frac{\int_0^z |\mathcal{E}^*|^2 dx}{\int_{-\infty}^{\infty} |\mathcal{E}^*|^2 dx}. \quad (36)
 \end{aligned}$$

The term involving the integration with respect to  $x$  gives the fraction of the air mode radiated into the air. Furthermore, the boundary conditions require that

$$h^+(\rho, z=0) = 0$$

$$\Rightarrow h^+ = -\frac{1}{2i\beta} \int_0^z H(\rho, \xi) d\xi$$

$$h^-(\rho, z=L) = 0 \quad (37)$$

$$h^- = \left[ \frac{1}{2i\beta} \int_L^z \exp(-2i\beta\xi) H(\rho, \xi) d\xi \right] \exp(2i\beta z). \quad (38)$$

Using the previous conditions and (32), (12), and (20), we get

$$h^+(\rho, L) = \frac{k^2(n_1^2 - n_2^2)}{4i\omega\mu P} \phi_+ AC_r \quad (39)$$

$$h^-(\rho, 0) = \frac{k^2(n_1^2 - n_2^2)}{4i\omega\mu P} \phi_- AC_r \quad (40)$$

where

$$\phi_+ = \phi_+(\beta, L) = \int_0^L f(z) \exp(i(\beta - \beta_0)z) dz \quad (41)$$

and

$$\phi_- = \phi_-(\beta, L) = \int_0^L f(z) \exp(-i(\beta + \beta_0)z) dz. \quad (42)$$

Using (19) and (26) we can calculate  $h^+(\rho, L)$ , namely

$$\begin{aligned}
 |h^+(\rho, L)|^2 = & \frac{k^4(n_1^2 - n_2^2)^2 |\phi_+|^2 \kappa_0^2}{|\beta_0| [d + 1/\gamma_0 + 1/\delta_0] (\kappa_0^2 + \delta_0^2) \pi |\beta|} \\
 & \cdot \left[ (\cos \sigma d - F_1 \sin \sigma d)^2 + \frac{\sigma^2}{\rho^2} (\sin \sigma d \right. \\
 & \left. + F_1 \cos \sigma d)^2 + \left( 1 + \frac{\sigma^2}{\Delta^2} F_1^2 \right) \frac{\Delta}{\rho} \right]^{-1} \quad (43)
 \end{aligned}$$

where  $\kappa_0$ ,  $\gamma_0$ ,  $\delta_0$  refer to the zero-order-mode solutions for (15)-(18).

Similarly

$$|h^-(\rho, 0)|^2 = \frac{|h^+(\rho, L)|^2 |\phi_-|^2}{|\phi_+|^2}. \quad (44)$$

Finally, to calculate the fraction of the air mode radiated into air, we use (20)-(22)

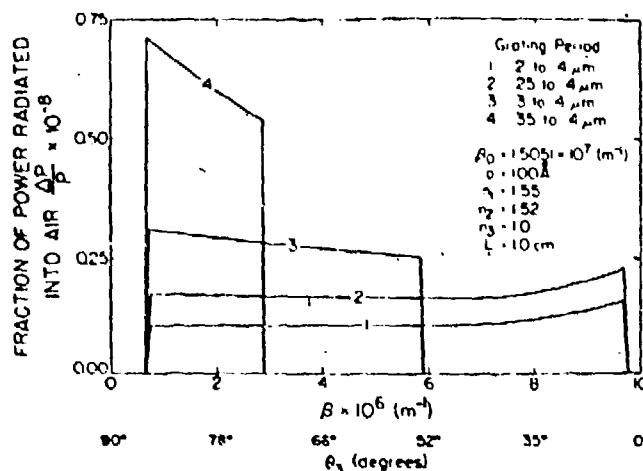


Fig. 9. Fraction of mode power radiated into air per unit  $\beta$  as a function of  $\beta$  or  $\theta_3$ , where  $\theta_3$  is the angle of scattering with respect to the  $z$  axis (see Fig. 6) for various chirps. The area under each curve represents the total power radiated into air for a given chirp.

$$\left( \frac{\int_0^{\pi} |\mathcal{E}^a|^2 dx}{\int_0^{\pi} |\mathcal{E}^i|^2 dx} \right)_{\text{even}}^{\text{odd}} = \frac{1 + (\sigma^2/\Delta^2) F_i^2}{1 + u_i^2 + w_i^2 + (\sigma^2/\Delta^2) F_i^2} \quad (45)$$

where

$$u_i = \cos \sigma d - F_i \sin \sigma d \quad (46)$$

$$w_i = \frac{\sigma}{c} (\sin \sigma d + F_i \cos \sigma d). \quad (47)$$

Now, using (45)-(43), (36) becomes

$$\left( \frac{\Delta P}{P} \right)_{\text{radiated into air per unit } \beta} = \frac{S}{\rho} [|\phi_+|^2 + |\phi_-|^2] \cdot \sum_{i=1}^2 \frac{u_i}{[(v_i)^2 + (w_i)^2 + u_i] \cdot [(v_i)^2 + (w_i)^2 + \frac{\Delta}{\rho} u_i]} \quad (48)$$

where

$$u_i = 1 + \frac{\sigma^2}{\Delta^2} F_i^2 \quad (49)$$

and

$$S = \frac{k^4 (n_1^2 - n_3^2) \kappa_0^2}{|\beta_0| (d + 1/\gamma_0 + 1/\delta_0) (\kappa_0^2 + \delta_0^2) \pi} \quad (50)$$

Equation (48) shows the fractional power radiated per unit beta for an arbitrary perturbation on the top surface. Once the perturbation is given, then  $\phi_+$  and  $\phi_-$  can be calculated.

For the particular case of the chirped grating with a transmission function given by (4),  $f(x)$  can be written as

$$f(x) = a \sin(\alpha x + \gamma x^2). \quad (51)$$

Direct substitution into (41) and (42) and using the method of stationary phase results in

$$|\phi_+|^2 = \frac{\pi a^2}{4\gamma} \quad (52)$$

if

$$\gamma > 0 \quad \alpha + \beta - \beta_0 < 0 \quad \alpha + \beta - \beta_0 + 2\gamma L > 0 \quad (52a)$$

or

$$\gamma < 0 \quad \alpha + \beta - \beta_0 > 0 \quad \alpha + \beta - \beta_0 + 2\gamma L < 0 \quad (52b)$$

or

$$\gamma < 0 \quad \alpha + \beta_0 - \beta > 0 \quad \alpha + \beta_0 - \beta + 2\gamma L < 0 \quad (52c)$$

otherwise  $\phi_+ = 0$ .

Similarly,

$$|\phi_-|^2 = \frac{\pi a^2}{4\gamma} \quad (53)$$

if

$$\gamma > 0 \quad \alpha - \beta - \beta_0 < 0 \quad \alpha - \beta - \beta_0 + 2\gamma L > 0 \quad (53a)$$

or

$$\gamma < 0 \quad \alpha - \beta - \beta_0 > 0 \quad \alpha - \beta - \beta_0 + 2\gamma L < 0 \quad (53b)$$

or

$$\gamma < 0 \quad \alpha + \beta + \beta_0 > 0 \quad \alpha + \beta + \beta_0 + 2\gamma L < 0 \quad (53c)$$

otherwise  $|\phi_-|^2 = 0$ .

These conditions, (52a)-(52c) and (53a)-(53c), give the range of  $\beta$  for which the guide radiates.

To illustrate (48), we present Fig. 9. The guide is 1.0 cm long, its thickness is  $0.6425 \mu\text{m}$ , and the index of refraction is  $n_1 = 1.55$ . The substrate index of refraction is  $n_2 = 1.52$ , and that of air is taken to be  $n_3 = 1.0$ . The film perturbation is of the form of (51) and  $a$  was chosen to be  $0.01 \mu\text{m}$ . The calculation for the fundamental mode gave  $\beta_0 = 1.505 \times 10^7 \text{ m}^{-1}$  corresponding to a wavenumber of  $9.78 \times 10^6 \text{ m}^{-1}$ . The figure illustrates the fractional power output in the air per unit  $\beta$  as a function of  $\beta$  for various chirps. We see from the

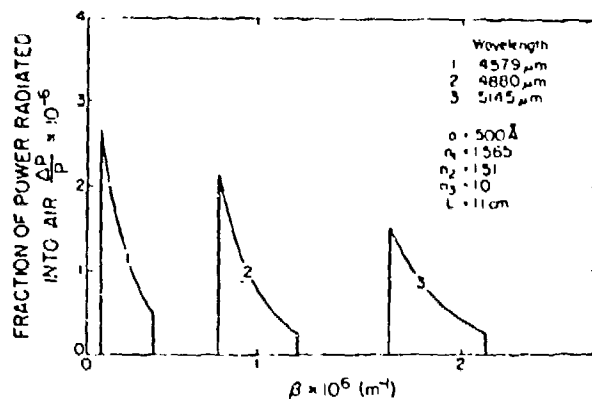


Fig. 10. Fraction of mode power radiated into air per unit  $\beta$  as a function of  $\beta$  for a chirp of 0.33-0.295  $\mu\text{m}$  and various wavelengths. The amplitude of the chirp is set at 500  $\text{\AA}$ , and the corrugation extends over a length  $L$  of 1.1 cm.

figure that the lower the chirp (curve 4) the narrower the range of  $\beta$  distribution. In the limit of no chirp, we expect the familiar  $\delta$ -function. For high chirp we have a wide range of  $\beta$  distribution extending over most of the theoretically possible range ( $k_x = 0$  to  $k$ ). The total power output radiated into air is the area under the curves. For Fig. 9, it ranges from 10 to 15 percent of the incident-mode power.

It is important to note that in the actual calculation the waveguide is divided into approximately one hundred sections.  $\Delta P/P$  is calculated from the first section and then it is subtracted from the total  $P$ . This new value of  $P$  is used as input power for the next section, and so on. This enables us to handle large power coupling and not be limited by the first Born approximation. This particular point is illustrated in Fig. 10. The total power output radiated into air is greater than 45 percent, due to the larger perturbation. In Fig. 10 the film thickness is 1.35  $\mu\text{m}$  and its index of refraction  $n_1 = 1.565$ . The substrate has an index of refraction  $n_2 = 1.51$  and air  $n_3 = 1.0$ . The guide is 1.1 cm long and again the perturbation on the top surface is given by (51). In this case,  $a$  is 0.05  $\mu\text{m}$ , and the period varies from 0.295 to 0.33  $\mu\text{m}$ . The different curves represent the fractional power output per unit  $\beta$  for various wavelengths. It can be seen from this figure that different wavelengths radiate over different and nonoverlapping  $\beta$  ranges.

In addition, we have calculated the fractional power (per unit  $\beta$  radiated into air and substrate) and found that, as predicted by the theory [9], it is twice as large as the one radiated into air.

## V. EXPERIMENTAL RESULTS

As a first demonstration of a device based on chirped gratings we chose a focusing output coupler. This grating coupler, with variable period, was corrugated on the surface of an optical waveguide, and was designated to focus the light a few centimeters away from the surface.

A layer of Corning 7059 glass which was sputtered on a glass substrate served as a waveguide. The 7059 glass was sputtered using Technics MIM Model 5.5 ion-beam etching machine, resulting in a layer of a refractive index of 1.565 and thickness uniformity of about 5 percent. For the focusing experiment

we deposited a layer of thickness 1.35  $\mu\text{m}$  (as measured by a Sloan Dektak instrument).

Chirped gratings were fabricated on the surface of the waveguide as follows: a layer of undiluted Shipley AZ1350B photoresist was spin coated at 3600 rpm on the waveguide. After prebaking, the photoresist was exposed to the interference pattern of a collimated laser beam with a converging beam. As detailed above, such interference pattern gives rise to chirped gratings. We used the  $\lambda = 4579 \text{ \AA}$  line from an  $\text{Ar}^+$  laser, and under the following conditions  $\theta = 94.5^\circ$ ,  $F = 1.33$ ,  $L = 1.2 \text{ cm}$ , we obtained gratings with periods varying from 0.29 to 0.33  $\mu\text{m}$  over a distance of 1.2 cm.

Typically the laser beam intensity was 0.6  $\text{mW}/\text{cm}^2$  (in each leg) and the exposure time used was 60 s. Gratings of high efficiency were obtained using an AZ 303 developer and 10-s development time. It should be mentioned that the intensity of  $\text{Ar}^+$  lasers is usually inferior to that of He-Cd ones, and in our experiment we had to use a fringe-stabilization system in order to improve the peak-to-trough height of the photoresist gratings.

The photoresist was next postbaked under vacuum for 30 min, and the waveguide was ion-beam etched through the photoresist, at ion current density 0.1  $\text{mA}/\text{cm}^2$  and accelerating voltage of 1800 V, for 30 min. The sample was kept at an angle of  $30^\circ$  with respect to the ion beam. The gratings thus fabricated in the glass had a peak-to-trough height of about 500  $\text{\AA}$ .

In the focusing experiment, we coupled light from an argon laser into the waveguide using a prism coupler. The light entering the corrugated section was focused outside the waveguide. The position of the focal point ( $x_f, z_f$ ) was measured experimentally for various lines of the argon laser. The experimental points are shown in Fig. 11, along with the theoretical predicted curve for this particular waveguide.

An output prism coupler was added at the end of the corrugated region. The light intensity which was coupled out was measured for two cases: a) light going through the corrugated region, and b) light going through a neighboring uncorrugated region. The ratio between the intensities in case a) and case b) was found to be 1:10.

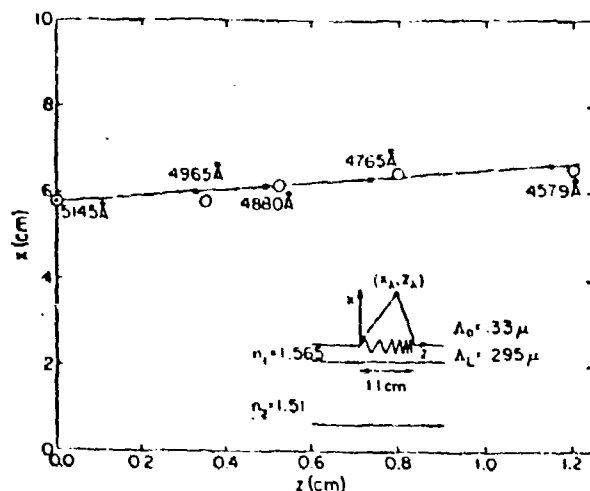


Fig. 11. Experimental and theoretical results of the focusing of the corrugated structure used. The solid line represents the theoretical position of the focus as a function of wavelength. The solid dots represent the focus of the prominent lines of the Ar<sup>+</sup> laser. The large circles are the experimental points for these wavelengths as measured with a two-dimensional translation probe.

## VI. DISCUSSION

In this work we have demonstrated first how chirped gratings can be fabricated in a photoresist layer by the interference of a collimated beam with a converging beam. We have calculated how the chirping varies with the various parameters of the experimental setup involved. As one important application of chirped grating, we demonstrated the focusing effect in a waveguide incorporating a chirped grating. The thickness of this waveguide and the chirp were chosen so as to focus the light about 6 cm away from the waveguide. The theoretical calculations, which were verified experimentally, show that the focal point moves by about 1.2 cm when the wavelength was changed from 4579 to 5145 Å. The chirped-grating structure therefore separates very well between propagating beams of different wavelengths, while focusing them outside the waveguide.

Other devices, which are based on chirped gratings, can also be realized. The first is a broad-band optical filter [10]. It is well known [12] that a grating structure with a period  $\Lambda$  will act as a selective reflector, and will reflect only wavelength  $\lambda$  that satisfies Bragg law  $\lambda/2n = \Lambda$ . The reflectivity can be rather high if the depth of the corrugations and if the length of the corrugated region are high. If the gratings have variable period  $\Lambda(z)$ , say between  $\Lambda_1$  and  $\Lambda_2$ , then all the wavelengths  $\lambda_2 > \lambda > \lambda_1$  will be reflected, provided  $\lambda_1 = 2n\Lambda_1$  and  $\lambda_2 = 2n\Lambda_2$ . The response of this broad-band filter (i.e., reflectivity versus wavelength) can be changed by changing the chirp. Such broad-band filters may well be incorporated as reflectors in corrugated laser structures such as DFB lasers [3] or DBR lasers [4].

Another device, which may have a significant importance is a beam splitter. It was shown [10] that if a guided beam of wavelength  $\lambda$  is incident on a corrugated region with an incidence angle  $\alpha$ , the beam will be deflected at an angle  $2\alpha$ , provided  $\lambda/2n \cos \alpha = \Lambda$ , where  $\Lambda$  is the period and  $n$  is the

refractive index of the waveguide. The fraction of the intensity that is deflected depends again on the corrugation depth and the length of the corrugated region. If the corrugated region consists now of chirped gratings with variable period  $\Lambda(z)$ , then a particular wavelength  $\lambda_1$  will be reflected from a particular region where the period  $\Lambda_1$  satisfies Bragg's law  $\Lambda_1 = \lambda_1/2n \cos \alpha$ .

A different  $\lambda_2$  will be reflected by  $\Lambda_2$ , so that  $\Lambda_2 = \lambda_2/2n \cos \alpha$ . Actually,  $\lambda_1 = \lambda(z_1)$  and  $\lambda_2 = \lambda(z_2)$ , so that the two wavelengths will be reflected from different regions, and they will be separated spatially. And, therefore, if we have a beam that consists of many wavelengths  $\lambda_i$ , the chirped-grating structure will demultiplex it. It is conceivable by this method to demultiplex a signal traveling in a fiber, and to send each frequency component to a different fiber. If the directions of the previously mentioned beams are reversed, the chirped grating structure will act as a multiplexer. Beams of different frequencies will be reflected now to a common direction, and could then be focused into a single fiber. Such multiplexing and demultiplexing experiments are now in progress in our laboratory.

Chirped-gratings structures will undoubtedly be useful not only in integrated optics but in other fields. One important field is that of surface acoustic waves, where gratings with variable periods have been made using electron-beam writing [11].

## ACKNOWLEDGMENT

The authors wish to thank Prof. N. George for many helpful discussions, and D. R. Armstrong and P. Agmon for their assistance.

## REFERENCES

- [1] A. Yariv and M. Nakamura, "Periodic structures for integrated optics," *IEEE J. Quantum Electron.*, this issue, pp. 233-253.
- [2] D. C. Flanders, H. Kogelnik, R. V. Schmidt, and C. V. Shank, "Grating filters for thin film optical waveguides," *Appl. Phys.*

- Lett.*, vol. 24, p. 194, 1974.
- [3] K. Aiki, *et al.*, "GaAs-GaAlAs distributed feedback diode lasers with separate optical and carrier confinement," *Appl. Phys. Lett.*, vol. 27, p. 145, 1975.
- [4] W. Ng, H. W. Yen, A. Katzir, I. Samki, and A. Yariv, "Room temperature operation of GaAs Bragg Mirror lasers," *Appl. Phys. Lett.*, vol. 29, p. 684, 1976.
- [5] M. L. Dakas, L. Kuhn, P. F. Heidrich, and B. A. Scott, "Grating coupler for efficient excitation of optical guided waves in thin films," *Appl. Phys. Lett.*, vol. 16, p. 523, 1970.
- [6] R. A. Bartolini, "Characteristics of relief phase holograms recorded in photoresists," *Appl. Opt.*, vol. 13, p. 129, 1974.
- [7] D. Marcuse, "Mode conversion caused by surface imperfections of a dielectric slab waveguide," *Bell Syst. Tech. J.*, vol. 48, p. 3187, 1969.
- [8] —, *Theory of Dielectric Optical Waveguides*. New York: Academic, 1974.
- [9] W. Streifer, R. D. Butnham, and D. R. Scifres, "Analysis of grating-coupled radiation in GaAs:GaAlAs lasers and waveguides—II: Blazing effects," *IEEE J. Quantum Electron.*, vol. QE-12, p. 494, 1976.
- [10] H. Kogelnik, "Filter response of nonuniform almost-periodic structures," *Bell Syst. Tech. J.*, vol. 55, p. 109, 1976.
- [11] K. S. Pennington and L. Kuhn, "Bragg diffraction beam splitter for thin film optical guided waves," *Opt. Commun.*, vol. 3, p. 387, 1971.
- [12] R. C. Williamson, "Properties and applications of reflective-array devices," *Proc. IEEE*, vol. 64, p. 702, 1976.

## Chirped-grating demultiplexers in dielectric waveguides\*

A. C. Livanos, A. Katzir, A. Yariv, and C. S. Hong

California Institute of Technology, Pasadena, California 91125

(Received 17 January 1977; accepted for publication 14 March 1977)

A wavelength-selective beamsplitter has been realized by fabricating chirped (variable period) grating in an optical waveguide. This beamsplitter can demultiplex a signal traveling in a fiber and send each frequency component to a different fiber.

PACS numbers: 42.80.Hq, 42.80.Lt, 42.60.Fc

We have recently described the fabrication of chirped (variable period) gratings in dielectric waveguides<sup>1</sup> and have demonstrated the use of these gratings in fabricating focusing output couplers.<sup>2</sup> In this work we report the use of chirped gratings for the realization of multiplexing or demultiplexing devices.

Consider a dielectric waveguide with a corrugated region of period  $\Lambda$ , and a guided optical beam of wavelength  $\lambda$  incident on the corrugated region at an angle  $\alpha$  [see Fig. 1(a)]. The beam will be deflected<sup>3</sup> at an angle  $2\alpha$ , provided Bragg's law  $\Lambda = \lambda/2n \cos \alpha$  is satisfied, where  $n$  is the effective refractive index of the waveguide.

If the corrugated region consists of a grating with a variable period  $\Lambda(z)$ , then it follows that different locations in the corrugated waveguide will deflect different wavelengths as shown in Fig. 1(b). A particular wavelength  $\lambda_1$  will be reflected from that part of the chirped grating where the period  $\Lambda_1$  satisfies the condition  $\Lambda_1 = \lambda_1/2n \cos \alpha$ , while a (different) wavelength  $\lambda_2$  will be reflected from the portion of the grating where the period  $\Lambda_2$  satisfies the condition  $\Lambda_2 = \lambda_2/2n \cos \alpha$ . These two wavelengths, which initially occupy the same beam, are thus demultiplexed, i. e., separated spatially. The fraction of the light of wavelength  $\lambda_1$  that is reflected depends on the length of the waveguide section for which

the wavelength  $\lambda_1$  falls within the "forbidden" propagation gap. It is thus a function of the chirp rate and the coupling constant, which in a given waveguide depends on the corrugation height and profile.

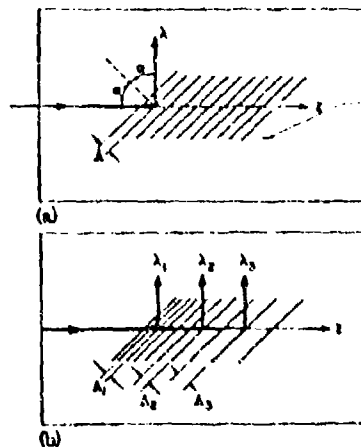


FIG. 1. (a) Beamsplitting in a dielectric waveguide with a constant grating period  $\Lambda$ . (b) Beamsplitting and demultiplexing in a dielectric waveguide with chirped [variable period  $\Lambda(z)$ ] grating.

To fabricate waveguides we used an ion-milling system, and sputter deposited a waveguiding layer of 7059 Corning glass on No. 3010 Clay-Adams microscope slides. The samples were cleaned according to the method described in Ref. 4, and the back surface was painted flat black. A layer of AZ-1350B photoresist was then deposited, and after 30 sec was spun at 3600 rpm for 30 sec. This was followed by baking for 30 min at 125 °C.

The chirped grating was recorded in the photoresist by exposing the latter to the interference pattern of a collimated laser beam with a converging one, generated by a cylindrical lens. The chirping depends on the angle between the illuminating beams, the wavelength, the  $F$  number of the lens, and the position of the lens with respect to the sample.<sup>1</sup>

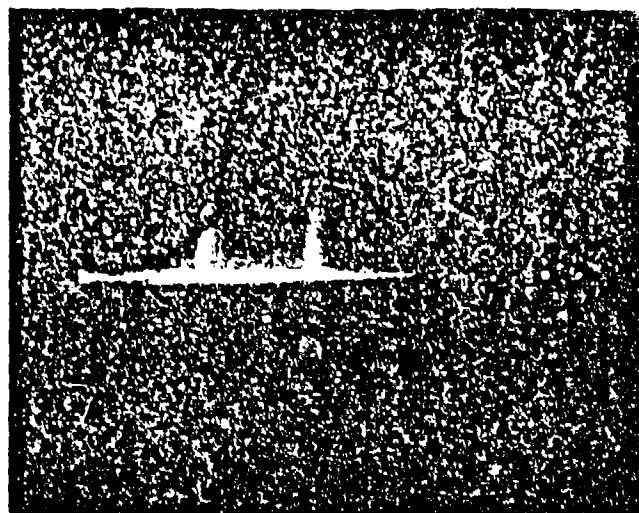
For this experiment we used an Ar<sup>+</sup> laser at the 4579-Å line. The angle between the collimated beam and the bisector of the converging beam was 95°. The  $F$  number of the lens was chosen to be 2.66 and the pattern was recorded over a distance of 9 to 14 mm. This arrangement resulted in a total period variation of 8 to 10% over the grating length. The samples were exposed for 65 sec and the power per beam was 1.2 mW/cm<sup>2</sup>. Subsequently they were developed for 10 sec in AZ-303A developer and rinsed for 2 min in deionized water. They were vacuum baked at 100 °C for 30 min, and then the chirped-grating pattern was transferred onto the waveguides using the same ion-milling machine.

In the first experiment reported here we have used a single mode waveguide of thickness 0.95 μm, as measured at a number of points by a Sloan Dektak machine. The thickness uniformity was better than 15%. The total period variation of the chirped grating was 2930 to 3210 Å over a distance of 6.5 mm, normal to the grating lines, and it was determined from the diffraction angle of an externally incident Ar<sup>+</sup> laser beam. The peak-to-trough height of the corrugations in the glass was approximately 500 Å.

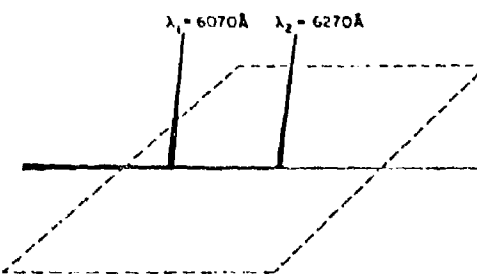
In the demonstration of wavelength demultiplexing we launched the tunable output beam of a cw dye laser into the waveguide using a prism coupler. The angle  $\alpha$  between the propagating beam and the grating was adjustable, and was chosen to be approximately 48°.

It was found that for yellow light, the light is reflected from the left side of the chirped grating, and as the wavelength increases the reflected beam moves to the right. The reflection at two distinct wavelengths 6070 and 6270 Å is shown in Fig. 2(a). These beams are separated spatially by 4 mm. Figure 2(b) shows the outline of the grating, as well as the positions of the reflected beams.

To measure more quantitatively the  $x$  coordinate of the location where reflection occurred as a function of wavelength, a second experiment was performed. A 0.65-μm waveguide with surface uniformity better than 5% was used. The effective index of refraction of the waveguide was measured with conventional prism coupling methods and was found to be  $1.53 \pm 0.01$ . The



(a)



(b)

FIG. 2. (a) Double-exposure photograph showing the reflection of two different wavelengths from two different locations in a chirped-grating beamsplitter. (b) Schematic representation of the experiment shown in Fig. 2(a). The dashed lines outline the corrugated region and the solid ones outline the laser beams.

period variation as a function of distance was measured as before and was found to vary from 2975 to 3360 Å over the total distance of 9.9 mm. This variation was linear over the region of interest of 3.5 mm and ranged from a low of  $2975 \pm 10$  Å to a high of  $3105 \pm 10$  Å. By measuring the diffraction efficiency of the Ar<sup>+</sup> beam used, the peak-to-trough height of the grating was estimated to be 400 Å. The angle  $\alpha$  between the incident beam and the grating was measured to be  $50^\circ \pm 1^\circ$ .

The dye laser was tuned from 6030 to 6300 Å and the locations of the reflection of different wavelengths were determined by using a traveling telescope mounted on a translation stage. Since the period variation  $\Lambda$  as a function of  $x$  was already known, we could now correlate the wavelength  $\lambda$ , and the period  $\Lambda$ , that caused reflection. The plot of  $\lambda$  as a function of  $\Lambda$  is shown in Fig. 3.

The first line plot of  $\Lambda$  versus  $\lambda$  agrees with Bragg's law  $\Lambda = \lambda/2n \cos \alpha$ . From the slope of the line and the measured incidence angle  $\alpha = 50^\circ \pm 1^\circ$  we calculate an effective index of refraction  $n = 1.5 \pm 0.1$  in agreement with the value determined, independently, by the prism coupling method.

As a rough estimate of the reflection at a given wavelength we use the expression for the power reflection

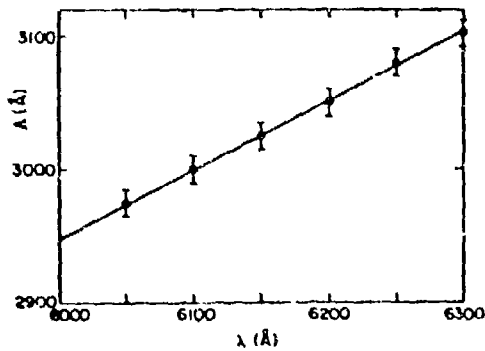


FIG. 3. The dependence of reflected wavelength  $\lambda$  on the period  $\Lambda$  at the reflection region. The straight line plot agrees with Bragg's law  $\Lambda = \lambda/2n \cos \alpha$ .

at the Bragg condition from a corrugated section of length  $L$  of a dielectric waveguide

$$R = \tanh^2(\kappa_l L), \quad (1)$$

where  $\kappa_l$  is the Bragg  $l$ th-order coupling constant.<sup>5</sup> In the case of a corrugated waveguide we replace  $L$  by  $L_{\text{eff}}$  which is taken as the length of the waveguide section in which the period  $\Lambda(x)$  falls within the forbidden propagation gap. The range of  $\Lambda$  which is within the forbidden gap is

$$(\Delta\Lambda)_B = \frac{\kappa_l \lambda^2 l}{8\pi n^2 \cos^3 \alpha}. \quad (2)$$

Assuming a linear chirp

$$\Lambda(x) = \Lambda_0 + \alpha x, \quad (3)$$

we find that the distance over which the period varies by  $(\Delta\Lambda)_B$  is

$$L_{\text{eff}} = \frac{\kappa_l \lambda^2 l}{8\pi n^2 \cos^3 \alpha} \quad (4)$$

which when substituted in Eq. (1) gives

$$R \approx \tanh^2 \frac{\kappa_l^2 \lambda^2 l}{8\pi n^2 \cos^3 \alpha} \quad (5)$$

for the reflectivity at  $\lambda$ .

From the corrugation depth and the waveguide parameters we obtain  $\kappa_1 \approx 100 \text{ cm}^{-1}$ ,  $\alpha \approx 2 \times 10^{-6}$  which leads to  $R \approx 0.50$ . This value does not clash with the visual observation of roughly equal power splitting by the grating. Quantitative determination of  $R$  was thwarted by excessive waveguide scattering. An examination of Eq. (4) shows that in practice values of  $R$  between zero and unity are obtainable by controlling the coupling constant  $\kappa$  and the chirp constant  $\alpha$ . We note that  $\kappa_l$  is a decreasing function of  $l$  (typically  $\kappa_l \propto l^{-1}$ ) so that the reflection will tend to decrease with increasing Bragg order.

In this work we demonstrated the fabrication of a chirped-grating beamsplitter in an optical waveguide. The beamsplitter reflects light in the plane of the waveguide, and separates spatially beams of different wavelengths. As a device, this beamsplitter can demultiplex, according to wavelength, a signal traveling in a fiber, and send each frequency component to a different fiber or detector. If the directions of the beams are reversed, the same beamsplitter can be used for multiplexing, thus combining beams of different frequencies into a single beam.

\*Research supported by the Air Force Office of Scientific Research

<sup>1</sup>A. Katzir, A. C. Livanos, J. B. Shellan, and A. Yariv, IEEE J. Quantum Electron. (to be published).

<sup>2</sup>A. Katzir, A. C. Livanos, and A. Yariv, Appl. Phys. Lett. 30, 225 (1977).

<sup>3</sup>K. S. Pennington and L. Kuhn, Opt. Commun. 3, 357 (1971).

<sup>4</sup>S. L. Norman and M. P. Singh, Appl. Opt. 14, 818 (1975).

<sup>5</sup>A. Yariv, IEEE J. Quantum Electron. QE-9, 819 (1973).

## Linearity and enhanced sensitivity of the Shipley AZ-1350B photoresist

A. C. Livanos, A. Katzir, J. B. Shellan, and A. Yariv

The properties of the Shipley AZ-1350B positive photoresist used with the Shipley AZ-303A developer were investigated. It was found that the use of AZ-303A developer results in a significant improvement of the sensitivity and the linearity of the photoresist. The unexposed etch rate of the photoresist was  $35 \text{ \AA} \pm 5 \text{ \AA/sec}$ . Gratings of high efficiency have been successfully fabricated using the above combination of photoresist and developer.

Current work in integrated optics requires the fabrication of relief grating structures on photoresist and the subsequent chemical or ion beam etching through the photoresist.<sup>1</sup> If the period of the grating is to be less than  $0.4 \text{ \mu m}$  the Shipley AZ-1350B photoresist is commonly used. The properties of this positive acting photoresist have been examined in detail,<sup>2,3</sup> and it was found that the photoresist exhibits strong nonlinearity, especially for etch depth ranging from  $0.05 \text{ \mu m}$  to  $0.2 \text{ \mu m}$ . Bartolini<sup>4,5</sup> first showed that a different developer, namely the AZ-303A, used with the old AZ-1350 photoresist (now replaced by the 1350B) results in an unexposed resist etch rate of approximately  $200 \text{ \AA/sec}$ , removes the nonlinearity, and improves the sensitivity by a factor of 2 or 3. Linearity and speed or sensitivity are always of practical interest.<sup>6,7</sup> Norman and Singh<sup>8</sup> have studied the characteristics of the AZ-1350J resist (which has replaced the old AZ-1350H) used with the AZ-303A developer and report results similar to the ones presented in Ref. 5. It is the purpose of this paper to show that the AZ-303A developer can be used with the AZ-1350B photoresist resulting in improved sensitivity and linearity and unexposed resist etch rate of  $35 \pm 5 \text{ \AA/sec}$ .

Bartolini<sup>5</sup> has shown that for a positive acting photoresist the following relationship exists between etch depth  $\Delta d$  and exposure  $E$  (in units of energy per unit area):

$$\Delta d = T[r_1 - \Delta r \exp(-cE)], \quad (1)$$

where  $T$  is the development time in seconds,  $c$  is the exposure constant characteristic of the photoresist,  $r_1$  is the rate of etching of exposed molecules,  $r_2$  is the rate

of etching of unexposed ones, and  $\Delta r = (r_1 - r_2)$ . If the term  $cE$  is much less than 1, Eq. (1) can be linearized as follows:

$$\Delta d \sim \Delta r T c E + r_2 T. \quad (2)$$

In this work we determined the parameters involved in Eq. (2) for the Shipley AZ-1350B photoresist used with the AZ-303A developer.

The samples used were NO. 3010 microscope slides made by Clay Adams, which, cut in half, resulted in a size of  $38 \text{ mm} \times 25 \text{ mm} \times 1 \text{ mm}$ . The samples were cleaned according to the method presented in Ref. 8, and for some experiments the back surface was painted black with 3M Nextel 101-C10 velvet coating. The AZ-1350B photoresist was then deposited in a single layer, and after 30 sec it was spun at 3600 rpm for 30 sec. The samples were baked, next, for 30 min at  $100^\circ\text{C}$ .

The first experiment involved the determination of the etch rate of the unexposed resist as a function of development time for various solutions of AZ-303A developer with distilled water. For this purpose the samples were half immersed in the developer for the required time, rinsed with deionized water for 2 min, and then baked under vacuum at  $100^\circ\text{C}$  for 30 min. The step size was measured using a Sloan Dektat instrument, and the results are shown in Fig. 1. The 4:1 solution (four parts distilled water, 1 part AZ-303A developer) gave unacceptably high etch rates, and the 8:1 gave low and nonlinear ones. We chose the 6:1 dilution for all our experiments, since it exhibited a linear behavior and an acceptable etch rate of  $r_2 = 35 \text{ \AA} \pm 5 \text{ \AA/sec}$ . The development time chosen for the subsequent experiment was 10 sec.

For comparison, we performed the same experiment using the Shipley MF-312 developer. This developer is free from trace-metallic elements and is commonly used in the fabrication of photoresist gratings in semiconductor substrates. Figure 2 shows the unexposed etch rate as a function of development time in minutes for the manufacturer's recommended dilution of 1:1. In

The authors are with California Institute of Technology, Pasadena, California 91125.

Received 27 November 1976.

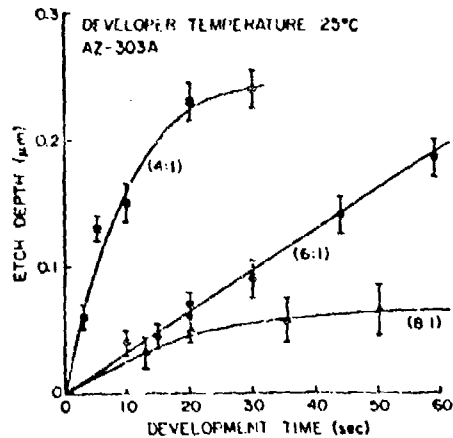


Fig. 1. Etch depths in  $\mu\text{m}$  of unexposed AZ-1350B photoresist as a function of development time in seconds for various dilution ratios of AZ-303A developer. The slope of the curves determines  $r_2$ , which for the 6:1 dilution is  $35 \text{ \AA} \pm 5 \text{ \AA}$ .

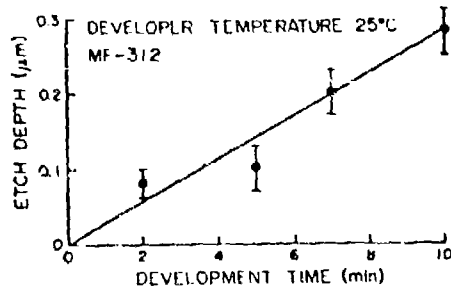


Fig. 2. Etch depth in  $\mu\text{m}$  of unexposed AZ-1350B photoresist as a function of development time in minutes for MF-312 developer. The 1:1 dilution results in  $r_2 = 5 \text{ \AA} \pm 1 \text{ \AA}$ .

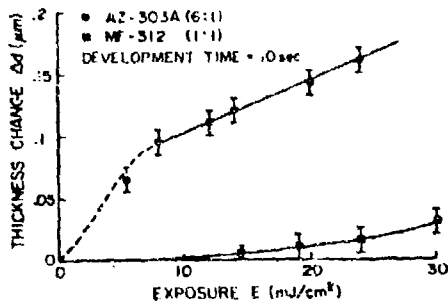


Fig. 3. Thickness change  $\Delta d$  in  $\mu\text{m}$  of AZ-1350B photoresist as a function of exposure  $E$  in  $\text{mW}/\text{cm}^2$ . The circles represent the AZ-303A developer, and the squares represent the MF-312 developer.

Table 1. Unexposed Etch Rate for AZ Photoresists and AZ-303A Developer

Photoresist	Unexposed etch rate	AZ-303A dilution	Reference
AZ-1350 replaced by AZ-1350B	150 $\text{\AA}/\text{sec}$	4:1	4,5
AZ-1350H replaced by AZ-1350J	35 $\text{\AA}/\text{sec}$	6:1	This paper
	200 $\text{\AA}/\text{sec}$	6:1	8

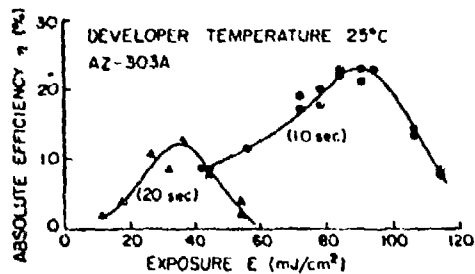
this case  $r_2$  is  $5 \text{ \AA} \pm 1 \text{ \AA}/\text{sec}$ , which is a much lower etch rate than the one for AZ-303A developer. If resist thickness is small, if long exposure times are acceptable, and if linearity is unimportant, this may indeed be a better choice.

The results for the different resists using the different dilutions of the AZ-303A developer are given in Table I.

To demonstrate the thickness change as a function of exposure time, the  $0.4416 \text{ }\mu\text{m}$  line of a He-Cd laser was used to illuminate half of the sample. The back surface of the sample was coated with black paint to avoid interference fringes. The intensity distribution of the laser was better than 5% across the surface of the sample. The photoresist was exposed for a given time and then developed 10 sec in the AZ-303A developer 6:1 dilution. Figure 3 shows the thickness change as a function of exposure energy. It can be clearly seen that the behavior of the photoresist in the important  $0.1\text{--}0.2\text{-}\mu\text{m}$  range is linear. In contrast, the MF-312 developer gave very small thickness changes for the same range of exposures. In order to verify that the stylus of the instrument was not scratching the surface, the same samples were aluminized and then tested.

To demonstrate the feasibility of using AZ-1350B photoresist with the AZ-303A developer in making high efficiency gratings, the following experiment was performed. Photoresist was spin-coated on samples at 3000 rpm, resulting in a resist thickness of about  $3.1 \text{ }\mu\text{m}$ . The gratings were generated by exposing the samples to the sinusoidal intensity distribution produced by the interference pattern of two collimated  $\text{Ar}^+$  laser beams. The wavelength used was  $0.4579 \text{ }\mu\text{m}$ , the angle between the beams  $94.5^\circ$ , and the intensity per beam  $0.60 \text{ mW}/\text{cm}^2$ . The exposed samples were developed in AZ-303A developer, baked under vacuum, and the efficiency of the gratings was measured. Figure 4 shows the absolute efficiency of the gratings as a function of exposure for two different development times. It is clear that high efficiency 23% resulted by developing the samples for 10 sec. To verify the theoretically predicted period and the peak to trough height, a scanning electron microscope was used. The period was measured to be  $0.31 \text{ }\mu\text{m}$ , and the peak to trough height was  $0.28 \text{ }\mu\text{m}$ .

The authors thank D. R. Armstrong for his valuable technical assistance. This research was supported by the U.S. Air Force Office of Scientific Research. The work of J. B. Shellan is supported in part by the Hertz Foundation.



4. Grating efficiency (absolute) as a function of exposure  $E$  in  $\text{mJ}/\text{cm}^2$  for 10-sec and 20-sec development times in AZ-303A developer. Initial resist thickness was  $0.31 \mu\text{m}$ .

In conclusion, we have found that the use of AZ-303A developer with the AZ-1350B photoresist results in an unexposed etch rate of  $\sim 35 \text{ \AA}/\text{sec}$  and significantly increases the sensitivity and linearity of the photoresist in the  $0.05\text{--}0.2\text{-}\mu\text{m}$  range. We have successfully made gratings with constant and variable period<sup>9</sup> using this method and have transferred them to glass using ion beam etching techniques.

#### References

1. H. L. Garvin, E. Garmire, S. Somekh, H. Stoll, and A. Yariv, *Appl. Opt.* **12**, 455 (1973).
2. S. Austin and F. T. Stone, *Appl. Opt.* **15**, 1971 (1976).
3. S. Austin and F. T. Stone, *Appl. Opt.* **15**, 2126 (1976).
4. R. A. Bartolini, *Appl. Opt.* **11**, 1275 (1972).
5. R. A. Bartolini, *Appl. Opt.* **13**, 129 (1974).
6. M. S. Htoo, *Photogr. Sci. Eng.* **12**, 169 (1968).
7. F. J. Loprest and E. A. Fitzgerald, *Photogr. Sci. Eng.* **15**, 260 (1971).
8. S. L. Norman and M. P. Singh, *Appl. Opt.* **14**, 818 (1975).
9. A. C. Livanos, A. Katzir, and A. Yariv, *Opt. Commun.* **20**, 179 (1977).

## Broad-band grating filters for thin-film optical waveguides<sup>2)</sup>

C. S. Hong, J. B. Shellan,<sup>b)</sup> A. C. Livanos,<sup>c)</sup> A. Yariv, and A. Katzir<sup>d)</sup>

California Institute of Technology, Pasadena, California 91125  
(Received 16 May 1977; accepted for publication 17 June 1977)

Broad-band grating filters have been fabricated on glass thin-film waveguides and evaluated with a tunable dye laser. Measured and calculated filter responses were found to be in good agreement. Grating filters with bandwidths of 300 and 150 Å, and reflectivities of 18 and 40%, respectively, are reported.

PACS numbers: 42.80.Cj, 42.80.Lt, 42.80.Fn, 42.52.+n

Gratings on the surfaces of thin-film optical waveguides have been used in a variety of applications such as couplers,<sup>1</sup> beam splitters,<sup>2</sup> and filters<sup>3,4</sup> in integrated optics. The grating with nonuniform period (chirped grating) has been the subject of current theoretical interest.<sup>5,6</sup> Recently chirped gratings fabricated on thin-film waveguides as output couplers<sup>7</sup> and wavelength demultiplexers<sup>8</sup> have been demonstrated.

In this work we report the use of chirped gratings for the realization of broad-band optical filters in thin-film waveguides. Chirped grating corrugations were fabricated on sputtered glass waveguides using the procedure described in Ref. 7. A tunable dye laser was used to measure the wavelength dependence of the filters' reflectivities. Bandwidths of 300 and 150 Å and reflectivities of 18 and 40%, respectively, were achieved. These values were in agreement with calculations based on measured waveguide and grating parameters.

Consider a thin-film waveguide supporting only the fundamental mode. A surface corrugation grating with a period equal to half the wavelength of the guided mode will cause the normally incident mode to undergo retroreflection.<sup>3</sup> The analysis of this problem uses the coupled-mode theory.<sup>3,9</sup> In a chirped grating whose period  $\Lambda$  varies as

$$2\pi/\Lambda(z) = 2\pi/\Lambda(0) - 2\gamma z, \quad 0 < z < L, \quad (1)$$

the coupled-mode equations become

$$\frac{dA}{dz} - i\delta A = -i\kappa B \exp(i\gamma z^2), \quad (2a)$$

$$\frac{dB}{dz} + i\delta B = i\kappa A \exp(-i\gamma z^2). \quad (2b)$$

$A$  and  $B$  are the complex amplitudes of the incident and reflected modes under consideration.  $\kappa$  is the coupling coefficient, which depends on the profile and the depth

<sup>1)</sup>Work supported by the National Science Foundation (Optical Communication Program) and the Air Force Office of Scientific Research.

<sup>2)</sup>Fannie and John Hertz Foundation Doctoral Fellow.

<sup>3)</sup>Present address: Hughes Research Laboratories, Malibu, Calif, 90265.

<sup>4)</sup>Present address: Physics Dept., Tel Aviv University, Tel Aviv, Israel.

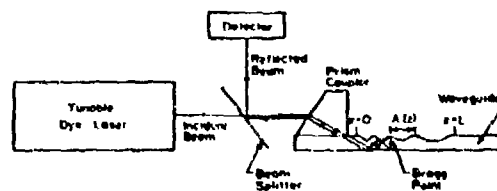


FIG. 1. Schematic of filter evaluation setup.

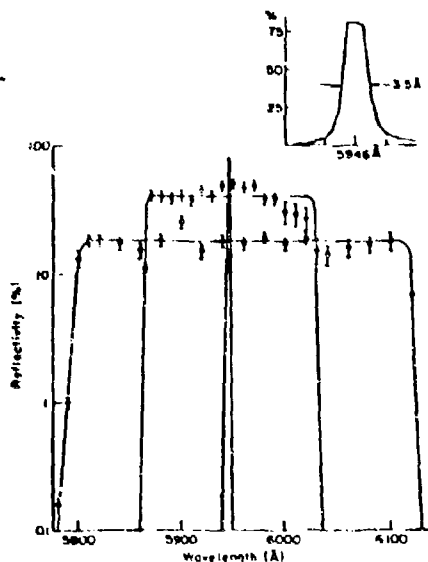


FIG. 2. Reflectivity versus wavelength for three grating filters.  $\circ$  represents filter 1;  $\times$  represents filter 2. A narrow-band filter (filter 3) is also shown and detailed in the inset.

of the grating corrugation.  $\delta$  is a phase mismatch factor and is defined by

$$\delta = \pi/\Lambda(z) - \beta, \quad (3)$$

where  $\beta$  is the propagation constant of the uncorrugated waveguide mode. The point where the Bragg resonance condition  $2\pi/\Lambda(z) - 2\beta = 0$  is satisfied shall be referred to as the Bragg point,  $z_B = \delta/\gamma$ . Equations (2a) and (2b) can be combined to give second-order differential equations for the incident wave  $A$  and the reflected wave  $R$ . The solutions of these equations are the parabolic cylinder functions.<sup>10</sup> By matching the boundary conditions for  $A$  and  $B$  and using the asymptotic expansions for the parabolic cylinder functions, we obtain the expression for reflectivity

$$R = 1 - \exp(-\pi\kappa^2/\gamma). \quad (4)$$

This asymptotic expansion is good for cases when the Bragg point is far from the grating edges, i. e.,  $5\kappa/\gamma < z_B < L - 5\kappa/\gamma$ .<sup>10</sup> However, for large chirps the incident mode is coupled into the reflected mode only over a portion of the grating length, and the resulting reflection may be small. Under these conditions we may set  $B=0$  in Eq. (2a), solve for  $A$ , and use this approximate solution of  $A$  in Eq. (2b) to solve for the reflected wave  $B$ . We account for residual waveguide losses by replacing  $\delta$  everywhere by  $\delta + \frac{1}{2}i\alpha$ , where  $\alpha$  is the (intensity)

loss constant.<sup>11</sup> Imposing the boundary condition  $B(L) = 0$ , the solution of Eq. (2b) using the approximation described above is

$$B(0) = -i \int_0^L \kappa(z) \exp(-i\gamma z^2) \exp[2i(\delta + \frac{1}{2}i\alpha)z] dz. \quad (5)$$

Carrying out the integration leads to a reflectivity

$$R = |B(0)|^2 \sim [\kappa(z_B)^2/\gamma] \exp(-2\alpha z_B) \quad \text{if } 0 < z_B < L \\ \approx 0 \quad \text{otherwise.} \quad (6)$$

In the experiment a glass waveguide was fabricated by sputter deposition of a layer of Corning 7059 glass on a glass substrate. A Shipley AZ-1350B photoresist film was spin coated on the waveguide. The chirped grating was recorded in the photoresist film by exposing the photoresist film to the pattern produced by the interference of a collimated laser beam and a cylindrically focused beam derived from the same laser. An Ar<sup>+</sup> laser line at 4579 Å was used. The exposure of the photoresist film took place inside a xylene bath, thus reducing the laser vacuum wavelength by 1.51, the index of refraction of xylene. Periods of  $\sim 1950$  Å were thus obtained. The  $F$  number of the cylindrical lens was chosen so that it resulted in a desired period variation over the grating surface whose length was 10 mm. The photoresist grating was then transferred to the waveguide surface by ion-beam etching. To evaluate the chirped grating filters, the output beam from a tunable dye laser (linewidth  $\sim 0.5$  Å) was launched into the waveguide by a prism coupler. This prism coupler also served as the output coupler for the reflected waveguide mode. The incident and reflected waves were separated by a beam splitter, and their relative power ratio was measured. The experimental setup is sketched in Fig. 1. In a chirped grating different wavelengths are reflected at different points along the grating. The light is launched into the short period end of the grating so as to minimize losses due to coupling into substrate radiation modes. As a result, longer wavelengths penetrate further into the grating and thus undergo a larger attenuation due to the residual waveguide loss. This loss  $\alpha$  was determined and the observed reflectivity at  $\lambda$  was multiplied by the factor  $\exp[2\alpha z_B(\lambda)]$  to obtain the intrinsic filter reflectivity. The loss-corrected spectral responses for two grating filters with different chirp factors are shown in Fig. 2. Also shown in Fig. 2 for comparison is the response of a uniform-period grating filter (1 mm long) whose band-limited characteristics is presented in the inset. The ability to tailor-design the bandwidth of an optical filter is thus manifest.

TABLE I. Summary of data obtained from three grating filters.

	Period (Å)	Length (L)	Corrugation depth (h)	Waveguide thickness (t)	Effective index of refraction at $\lambda = 5950$ Å <sup>a</sup>	Wavelength response	Bandwidth	Reflectivity	
Filter 1	Chirped	1905–2005 Å	10 mm	350 Å	0.77 μm	1.524	5810–6110 Å	300 Å	18%
Filter 2	Chirped	1825–1875 Å	10 mm	400 Å	0.85 μm	1.524	5870–6020 Å	150 Å	40%
Filter 3	Uniform period	1955 Å	1 mm	250 Å	0.80 μm	1.519	5946 Å	4 Å	80%

<sup>a</sup>  $n_x \sim 1.51$ ,  $n_y \sim 1.54$ ,  $n_z \sim 1$ .

The measured parameters of the three filters are summarized in Table I. The bandwidths are in good agreement with the design values, while the measured and calculated values of reflectivity are within 10%.

In conclusion, we have demonstrated the fabrication of chirped grating filters in thin-film optical waveguides. The control of the waveguide, corrugation, and chirp parameters leads to band rejection filters whose response conforms closely to design values.

The authors wish to acknowledge the assistance of D.R. Armstrong.

- <sup>1</sup>M. L. Dakes, L. Kuhn, P. F. Heidrich, and B. A. Scott, *Appl. Phys. Lett.* **16**, 523 (1970).
- <sup>2</sup>K. S. Pennington and L. Kuhn, *Opt. Commun.* **3**, 357 (1971).
- <sup>3</sup>H. Stoll and A. Yariv, *Opt. Commun.* **8**, 5 (1973).
- <sup>4</sup>D. C. Flanders, H. Kogelnik, R. V. Schmidt, and C. V. Shank, *Appl. Phys. Lett.* **24**, 194 (1974).
- <sup>5</sup>H. Kogelnik, *Bell Syst. Tech. J.* **55**, 109 (1976).
- <sup>6</sup>M. Matsuhara, K. O. Hill, and A. Watanabe, *J. Opt. Soc. Am.* **65**, 804 (1975).
- <sup>7</sup>A. Katzir, A. C. Livanos, J. B. Shellan, and A. Yariv, *IEEE J. Quantum Electron.* **QE-13**, 296 (1977).
- <sup>8</sup>A. C. Livanos, A. Katzir, A. Yariv, and C. S. Hong, *Appl. Phys. Lett.* **30**, 519 (1977).
- <sup>9</sup>A. Yariv, *IEEE J. Quantum Electron.* **QE-9**, 919 (1973).
- <sup>10</sup>R. B. Smith, *J. Opt. Soc. Am.* **66**, 882 (1976).
- <sup>11</sup>A. Yariv, *Quantum Electronics*, 2nd ed. (Wiley, New York, 1975), p. 520.

### Simultaneous exposure and development of photoresist materials: an analytical model

P. Agmon, A. C. Livanos, A. Katzir, and A. Yariv

When this work was done all authors were with California Institute of Technology, Pasadena, California 91125; A. C. Livanos is now with Hughes Research Laboratories, Malibu, California 90265 and A. Katzir is with Tel Aviv University, Physics Department, Tel Aviv, Israel.

Received 13 June 1977.

Positive photoresist plays an important role in fabricating a variety of devices, including diffraction gratings. The conventional method for making such gratings is to expose the photoresist to the interference pattern of two collimated laser beams, and then in a separate step to develop it. Tsang and Wang<sup>1</sup> proposed a new technique in which they exposed and developed the photoresist simultaneously. We shall refer to this technique as the SED (simultaneous exposure and development). This technique enabled them to reduce the exposure time and hence increase the SNR of the image in situations requiring large exposures. In addition they succeeded in producing gratings of deep grooves and narrow lines. In what follows, a simple analytic model for the SED method is described. The theoretical calculations are compared with experimental data.

Positive photoresist materials are composed of two major components: a base resin and a light-sensitive inhibitor compound. Photodecomposition of the inhibitor molecules during the exposure decreases its concentration and, as a consequence, increases the etching rate during development.

The rate at which the inhibitor concentration is reduced by

exposure to light can be described by<sup>2,3</sup>

$$\frac{\partial M(x,t)}{\partial t} = -\eta \frac{\alpha M(x,t) I(x,t)}{h\nu} \quad (1)$$

where

$x$  = depth in the photoresist film,  
 $M$  = inhibitor concentration ( $\text{cm}^{-3}$ ),  
 $I$  = light intensity,  
 $\eta$  = quantum efficiency,  
 $\alpha$  = absorption cross section of inhibitor molecules ( $\text{cm}^2$ ), and  
 $\nu$  = light frequency ( $\text{sec}^{-1}$ ).

Equation (1) can be rewritten

$$\frac{\partial M(x,t)}{\partial t} = -\frac{M(x,t)}{\tau(x,t)}, \quad (2)$$

where the decomposition time  $\tau$  is defined as

$$\tau(x,t) = \left[ \frac{\eta\alpha}{h\nu} I(x,t) \right]^{-1}. \quad (3)$$

$\tau$  is an important parameter: It contains the interaction between the light and the photoresist.

If we keep the source intensity constant and  $\alpha M(x,0)f \ll 1$ , where  $f$  is the film thickness, we may take  $I(x,t) \approx I_0$ . In this case  $\tau$  is independent of  $x$  and  $t$ , and Eq. (2) is easily solved. If the exposure starts at  $t = 0$ , then at  $t = T$

$$M(x,T) = M(x,0) \exp(-T/\tau) \quad (4)$$

In the conventional method during the development step, which follows the exposure, the photoresist is being etched at a rate which depends on the local inhibitor concentration. If the etching rate of unexposed photoresist is  $r_2(\mu\text{m}\cdot\text{sec}^{-1})$  and

that of fully bleached is  $r_1$  ( $\mu\text{m}\cdot\text{sec}^{-1}$ ), the development process can be modeled by

$$\frac{dx}{dt} = r_1 - \Delta r \frac{M(x,T)}{M(x,0)} \quad (5)$$

where  $\Delta r = r_1 - r_2$  and  $T$  = the exposure time. In the approximation of  $I(x,t) \approx I_0$ , Eq. (5) becomes<sup>2</sup>

$$L_D = [r_1 - \Delta r \exp(-T/\tau)]D \quad (6)$$

where  $L_D$  is the thickness of the photoresist layer removed during development time  $D$ .

In the SED technique a substrate coated with positive photoresist is immersed in the developer while exposed. As a result, the photoresist is exposed and etched simultaneously.

Following Eq. (5), the etching rate during SED is given by

$$\frac{dx}{dt} = r_1 - \Delta r \frac{M(x,t)}{M(x,0)} \quad (7)$$

which, for the approximation  $I(x,t) \approx I_0$ , becomes

$$\frac{dx}{dt} = r_1 - \Delta r \exp(-t/\tau) \quad (8)$$

If SED is started at  $t = 0$ , then at  $t = S$  the thickness of the photoresist layer which has been removed is

$$L_S = r_1 S - \Delta r \tau [1 - \exp(-S/\tau)] \quad (9)$$

If after following the SED step the exposure is turned off and the photoresist remains in the developer for a time  $D$  (i.e., conventional development), using Eq. (6), the thickness of the removed layer is

$$L_T = L_S + L_D = r_1 S + r_2 D + \Delta r [1 - \exp(-S/\tau)] (D - \tau) \quad (10)$$

The difference in height between the exposed and the unexposed areas is

$$\Delta L = L_T - r_2 (S + D) = \Delta r [S + (D - \tau) [1 - \exp(-S/\tau)]] \quad (11)$$

Defining  $s = S/\tau$ ,  $d = D/\tau$ ,  $\Delta l = \Delta L/\Delta r \tau$ ,

$$\Delta l = [s + (d - 1) [1 - \exp(-s)]] \quad (12)$$

Equation (12) describes the SED process and a following conventional development, independently of light intensity and developing parameters, provided Eq. (8) is valid.

To compare the theory with experimental data, Shipley 1350J positive photoresist in AZ-303A developer<sup>4</sup> was chosen. Earlier work by Bartolini<sup>2</sup> suggested that this photoresist-developer system satisfied Eq. (6) (for conventional exposure and development). A glass substrate coated with Shipley 1350J positive photoresist was immersed in AZ-303A developer, contained in a rectangular liquid gate with walls made of optically flat glass. The exposed region of the photoresist was uniformly illuminated by a  $4579 \text{ \AA}$  argon laser beam. The photoresist film thickness was initially  $5.0 \mu\text{m}$ . To compare experimental data with Eqs. (11) and (12) the plate was partially covered, such that only half of it was exposed to the laser light, while the whole plate (including the unexposed half) was immersed in the developer. As the plate was illuminated, the exposed half was simultaneously exposed and developed, while the covered half was developed only. The thickness difference between the two halves was measured using a Sloan Dektak instrument. The intensity used in the experiments was  $\sim 5.3 \text{ mW/cm}^2$  (on the photoresist) surface. The developer was diluted in a 1:6 ratio.<sup>5</sup>

For the theoretical calculations the values of  $\eta$ ,  $\alpha$ , and  $\Delta r$  are needed. Brody<sup>6</sup> has found  $\eta = 3.2\%$  and  $\alpha = 5.9 \times 10^{-17} \text{ cm}^2$  (measured at  $3654 \text{ \AA}$ ). Bartolini<sup>2</sup> has found  $\Delta r =$

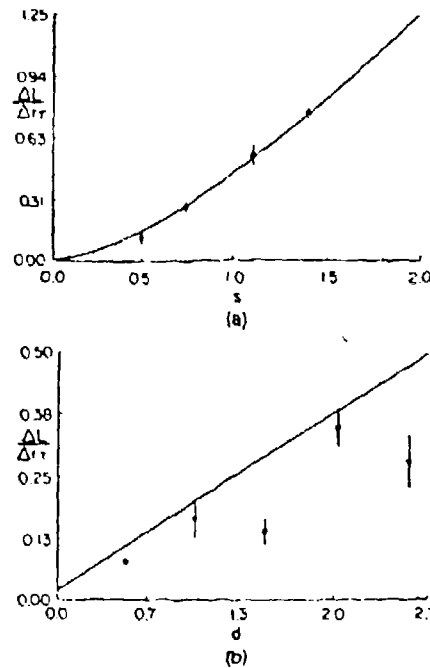


Fig. 1. Difference in etched depth between exposed and unexposed Shipley AZ-1350J photoresist in AZ-303A developer: (a) for varying SED time followed by constant conventional developing time ( $D = 5$  sec); (b) for constant SED time ( $S = 2.58$  sec) followed by varying conventional developing time. The solid lines are calculated using Eq. (12) with  $s = S/\tau$ ,  $d = D/\tau$ ,  $\tau = 37.7$  sec,  $I_0 = 5.3 \text{ mW/cm}^2$ ,  $\Delta r = 0.1 \mu\text{m/sec}$ .

$0.1 \mu\text{m/sec}$ . These values fit our measurements within the experimental error, and no effort was made to measure them directly.

The theoretical model and experimental data are compared in Fig. 1.

In Fig. 1(a) the SED duration is varied, while the conventional developing time is constant and small (5 sec, the time required to remove the sample from the liquid gate and rinse it in deionized water). This case is the most important one because it represents the regular use of SED. It is to be noted that here the agreement between theory and experimental data is good even when the removed layer is quite thick (for instance, the experimental point for  $s = 1.4$ , ( $\tau = 37.7$  sec,  $S = s\tau = 52.8$  sec) corresponds to  $\Delta L = 2.8 \mu\text{m}$  or total etched depth of  $L_T = 3.7 \mu\text{m}$ , using  $r_2 = 0.015 \mu\text{m/sec}$ ). In Fig. 1(b) the duration of the SED is constant and small while the following conventional developing time is varied. As expected, since the theoretical model does not take into account the nonuniform distribution of the light intensity through thickness of the photoresist, the theoretical prediction does not agree with the experimental points when the development time is long (thick photoresist layer).

The exposure energy and the etching rate as a function of depth can be calculated.

Consider a layer at depth  $x$  which is removed at  $t = S(x)$ . The exposure energy at that depth is

$$E(x) = \int_0^{S(x)} I(x,t) dt \approx I_0 S(x) \quad (13)$$

Define  $\epsilon(x) = E(x)/I_0 \tau$  and  $\xi = x/\Delta r \tau$ . Equation (13) becomes

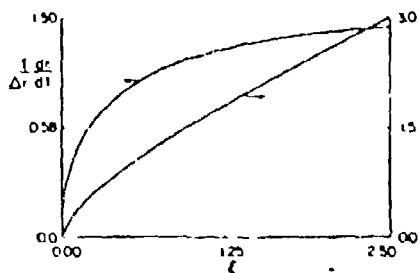


Fig. 2. Normalized etching rate  $[1/\Delta r/(dx/dt)]$  and exposure energy  $(\xi = E/I_0\tau)$  as a function of depth (using  $r_1/\Delta r = 1.15$ ).

$$\xi(\xi) = s(\xi). \quad (14)$$

From Eq. (9),

$$\xi = \left( \frac{r_1}{\Delta r} \xi(\xi) - [1 - \exp[-\xi(\xi)]] \right). \quad (15)$$

From Eq. (15) the exposure energy as a function of depth can be found. Once  $\xi(\xi)$  is known, it can be used, together with Eq. (14) and Eq. (8) to calculate the etching rate  $(dx/dt)$  as a function of depth.

The normalized exposure energy  $[\xi(\xi)]$  and etching rate

$$\left[ \frac{1}{\Delta r} \frac{dx}{dt}(\xi) \right]$$

are plotted in Fig. 2.

As is expected, in the SED process, both the exposure energy and the etching rate increase with depth, since each layer is exposed to radiation until it is etched. This is in contrast to the conventional method, where the deeper the layer the

smaller the exposure energy and, hence, the smaller the etching rate.

It is interesting, and important, to note that while in the conventional method the difference in etched depth between the exposed and unexposed photoresist is linear with the exposure time (and energy) for  $T/\tau < 1$  [see Eq. (6)], in the SED method it is linear with SED time for  $(S/\tau) > 1$ .

In conclusion, a simple analytic model was applied to the simultaneous exposure and development of positive photoresist. The model has been confirmed to be in good agreement with experiment under the following conditions.

1. Shipley 1350J positive photoresist in AZ-303A developer,
2. up to  $5 \mu\text{m}$  thickness of photoresist,
3. uniform illumination, and
4. short conventional developing time.

The validity of the model, for other types of photoresist/developer systems, is under investigation. In addition, its application to grating fabrication is studied.

The authors thank D. R. Armstrong for his assistance. This work was supported by the National Science Foundation, by the Office of Naval Research, and by the Air Force Office of Scientific Research.

#### References

1. W. T. Tsang and S. Wang, *Appl. Phys. Lett.* **24**, 196 (1974).
2. R. A. Bartolini, *Appl. Opt.* **13**, 129 (1974).
3. F. H. Dill, W. P. Hornberger, P. S. Hauge, and J. M. Shaw, *IEEE Trans. Electron Devices* **ED-22**, 445 (1975).
4. Shipley Company, Newton, Mass. 02162.
5. A. C. Livanos, A. Katzir, J. B. Shellan, and A. Yariv, *Appl. Opt.* **16**, 1635 (1977).
6. B. Broyde, *J. Electrochem. Soc.* **117**, 1555 (1970).

#### 4. Personnel Supported under the Subject Contract

##### 4.1 Professional Staff

Dr. Nicholas George, Principal Investigator

Dr. Alexander C.R. Livanos, Research Fellow

Mr. G.M. Morris, Graduate Student

Mr. M. Abushagur, Graduate Student

Mr. H. Parker, Graduate Student

Mr. M.J. Kavaya, Graduate Student

##### 4.2 Technician and Undergraduates

Mr. Joshua Rothenberg, Undergraduate

Mr. Everett Coffelt, Senior Technician

REPORT DOCUMENTATION PAGE		READ INSTRUCTIONS BEFORE COMPLETING FORM
1. REPORT NUMBER <b>AFOSR-TR-78-1506</b>	2. GOVT ACCESSION NO.	3. RECIPIENT'S CATALOG NUMBER
4. TITLE (and Subtitle) <b>OPTICAL DATA PROCESSING AND STATISTICAL OPTICS</b>		5. TYPE OF REPORT & PERIOD COVERED <b>FINAL</b>
		6. PERFORMING ORG. REPORT NUMBER
7. AUTHOR(s) <b>N. GEORGE</b>	8. CONTRACT OR GRANT NUMBER(s) <b>F49620 76-C-0021</b>	
9. PERFORMING ORGANIZATION NAME AND ADDRESS <b>California Institute of Technology Pasadena CA 91125</b>		10. PROGRAM ELEMENT, PROJECT, TASK AREA & WORK UNIT NUMBERS <b>61102F 2305B1</b>
11. CONTROLLING OFFICE NAME AND ADDRESS <b>AFOSR/NE Bolling AFB DC 20332</b>		12. REPORT DATE <b>Oct 78</b>
		13. NUMBER OF PAGES <b>41</b>
14. MONITORING AGENCY NAME & ADDRESS (if different from Controlling Office)		15. SECURITY CLASS. (of this report) <b>UNCLASSIFIED</b>
		15a. DECLASSIFICATION/DOWNGRADING SCHEDULE
16. DISTRIBUTION STATEMENT (of this Report)  <b>Approved for public release; distribution unlimited.</b>		
17. DISTRIBUTION STATEMENT (of abstract entered in Block 20, if different from Report)		
18. SUPPLEMENTARY NOTES	<b>YES</b>	
19. KEY WORDS (Continue on reverse side if necessary and identify by block number)		
20. ABSTRACT (Continue on reverse side if necessary and identify by block number) Research on the fabrication of grating structures for use in integrated optics is described. Chirped or variable period gratings have been successfully made by a holographic process. Briefly, a waveguiding layer of Corning 7059 glass is sputtered onto a substrate glass using the Technics MIM Model 5.5 ion beam etching machine. Photoresist is coated onto the waveguiding layer, exposed holographically in an argon or helium-cadmium laser beam, developed and then ion-milled. Extensive theory and technique are reported in the bibliography of publications listed in this report.		